Retardation of a sphere settling in a vertically oscillating fluid

DIPLOMA THESIS

submitted in partial fulfillment of the requirements for the degree of

Diplom-Ingenieur

in

Computational Science and Engineering

by

Benjamin Gruber

to

the faculty of
mechanical and industrial engineering

accepted on the recommendation of

Prof. Eckart Meiburg, UCSB
UC SANTA BARBARA

Prof. Alfredo Soldati, TU Wien
TU WIEN TECHNISCHE UNIVERSITÄT WIEN

February, 2024
Technische Universität Wien
A-1040 Wien ▪ Karlsplatz 13 ▪ Tel. +43-1-58801-0 ▪ www.tuwien.at

Erklärung zur Verfassung der Arbeit

Benjamin Gruber

Hiermit erkläre ich, dass ich diese Arbeit selbständig verfasst habe, dass ich die verwendeten Quellen und Hilfsmittel vollständig angegeben habe und dass ich die Stellen der Arbeit – einschließlich Tabellen, Karten und Abbildungen –, die anderen Werken oder dem Internet im Wortlaut oder dem Sinn nach entnommen sind, auf jeden Fall unter Angabe der Quelle als Entlehnung kenntlich gemacht habe.

Santa Barbara, 16. Februar 2024

Benjamin Gruber

Acknowledgements

I want to thank my supervisors, Prof. Alfredo Soldati who sparked my fascination for fluids and whose steady support I can rely on always and Prof. Eckart Meiburg whose curiosity inspired- and everlasting encouragement reassured me in my commitment to this fascinating problem.
Moreover many thanks to Alex Leonelli whose expertise and patience I could count on always (both in the lab and on the road-bike) and who I may now call friend.
Thank you to my family and friends who supported me in any way they could.
Finally, I am most grateful to the Austrian Marshall Plan Foundation, TU Wien and TU Wien's faculty for electrical engineering and information technology for funding- and the NSF-Access program for providing the computational resources for, this research.

Abstract

It has been shown that a particle settling through a vertically oscillating flow settles more slowly than through a quiescent fluid. The phenomenon is referred to as retardation and has found fruitful application in a multitude of industrial separation processes, such as in baffled tubes and jigs. While published experimental works partly document the influence of material properties (particle to fluid density ratio $\rho_s = \frac{\rho_p}{\rho_f}$, fluid kinematic viscosity ν) and flow characteristics (oscillation frequency f, ratio of amplitude to particle diameter $\frac{A}{D_p}$) on retardation, the mechanism behind slowed settling remains unclear. Furthermore, a universal law describing the retarded settling velocity remains unknown. To this end, a parametric study across the aforementioned material and flow properties is conducted by means of grain-resolved Direct Numerical Simulations (DNS). The fully resolved flow data around the oscillated particle obtained by this study allowed precise measurement and detailed description of the pressure and skin drag force. A strong link between retardation magnitude and the contribution of the pressure force F_{dp} to the net-lift was found. Differences in flow-structures during the particle's upward and downward-movement are brought forward, we suggest they are linked to an asymmetry in the pressure force F_{dp} increasing along retardation. Additionally, the influence of a horizontally confined domain on particle retardation was found to be significant. A novel dimensionless parameter is proposed for which a wide range of prior experimental data and simulation data obtained from this study collapse. Finally, levitation (infinitely suspended particle) as an extreme case of retardation was observed. However, the observation of this behaviour might be an artefact of geometric limitations.

Contents

CHAPTER 1

Prior work

1.1 Early contributions

Houghton [Hou63, Hou04, Hou04] was one of the first to develop theory describing decreased particle settling velocity in a vertically oscillating fluid field. They investigated both non-uniform "sawtooth" oscillations, where upward flow accelerations are greater than the downward flow accelerations, and symmetric sinusoidal oscillations of the flow. While the former have experimentally been shown capable of even transporting particles against gravity [Boy20, DK90, Bai03], the limit of the retarding effect on a single particle subjected to a uniformly sinusoidal velocity field remains unclear. The particle momentum balance Houghton modelled for the drag on the sphere did not include a Basset term (which allows for deviations of the flow pattern from that at steady state) and was therefore not affected by particle acceleration. Under the assumption of quasi-steady flow, where the drag coefficient is obtained from the instantaneous particle Reynolds number $Re_p = \frac{D_p u_p}{\nu}$, he arrived at a Mathieu equation, the solution of which suggested that combinations of amplitude and frequency existed for which levitation (suspension of the particle against gravitational force for an infinite amount of time) is attainable. Bailey [Bai03] concluded that (with driving frequency $f \to \infty$ and amplitude $A \to \infty$) the retardation effect due to symmetrical oscillation can be made strong enough to sustain levitation. They derived this from a model Bailey initially proposed for particle behaviour in piece-wise constant, asymmetrical flow. It is very close to a quasi-steady model by approximating the time integral over the Basset term as a constant.

1.2 Levitation in multi-particle systems

Inspired by a preceding experiment by Houghton, who successfully levitated an ensemble of glass beads in water, his student, Feinman [Fei01] experimentally explored levitation in systems of many particles. Houghton did not report on his observation, but Feinman mentioned it in the introduction of his own work. Experiments range over $Re = \frac{AD_p\omega}{\nu} = 60\text{-}2000$ and are based on a wide range of parameters ($f = 20\text{-}75Hz$ with $\omega = 2\pi f$, $\beta = 2\text{-}100$) and are conducted in either bromoform or water. He found that the volume fraction of the particle phase has a profound influence on particle retardation. He observed that in systems with large particle population,

single particles can be witnessed separating from the bunch and remain in levitation, however, it proved impossible to reproduce levitation for single particle systems or even systems that count only a few particles. He concluded that levitation of individual particles from the suspended bed depends on *"some kind of favorable initial conditions that result in a trajectory that can lead to stable levitation"*. For the specific oscillation column used in the study, they where able to demonstrate that for systems of more than 50 particles levitation effects became independent on the number of particles.

The only other work that puts forward levitation as an extreme form of particle retardation caused by symmetric flow oscillation is by Deng [DK90]. They did not report on particle velocities which is why we cannot establish a particle Reynolds number Re_p. However, levitation was observed in a water-glycerol mixture ($\nu \approx 1e^{-5}$) at $f = 15\text{-}30Hz$ and $\beta = 20$ yielding $Re = \frac{AD_p\omega}{\nu} \approx 200$. It is important to note that their experimental setup was also based on a multi-particle system and the authors failed to disclose information about the volume fraction. Lapple, who investigated the falling behaviour of single- and multi-particle systems [Lap56], found that increased drag on a settling sphere can arise through interference by other particles nearby. It is reasonable that oscillatory multi-particle systems are affected by similar effects. The notion of particle levitation and related concepts, such as levitation frequency (where for frequencies $f > f_{lev}$ particle levitation will occur for a fixed particle-fluid pair) made by Deng and critical levitation velocity by Feinman and Krantz [KCA11] should therefore not be used with respect to **uniformly** sinusoidal oscillated single-particle systems. In such systems particle levitation has no grounds in literature and the aforementioned concepts originate from research in multi-particle research. (For clarification: particle levitation in oscillating flow of the **non-uniform** sinusoidal- and 'sawtooth'-kind is well recorded [Hou63, Boy20, Bai03])

1.3 Physics of retardation

Back to single particle investigations: Baird [BST04] makes the interesting notion of minimum values of retardation (that is: there is an oscillatory intensity (he uses $fA^{\frac{1}{3}}$) at which maximum retardation is reached and beyond which the retardation effect will start to cease again). To explain his suggestion on retardation physics, we need to introduce vortex shedding: The wake that forms around a settling particle in a fluid at rest consists of a permanent vortex ring that oscillates and finally separates (sheds) periodically [Sch75] (that is in a regime that is characterized by a certain threshold particle Reynolds number Re_p). The natural vortex shedding frequency f_{nvs} describes the periodicity of shedding of the vortex and follows an empirical equation of the form $Sr_n = \frac{f_{nvs}D_p}{U_0} = \text{f}(Re_p)$, where U_0 is the settling velocity in a quiescent fluid and Sr_n is the natural Strouhal number [Ger66].

Baird suggests that oscillations imposed on the fluid can change a sphere's vortex shedding frequency f_{nvs} to the frequency of the oscillation f. Essentially, every change in direction made by the sphere (once per oscillation period T) causes shedding of the wake that has been built up during the oscillation cycle. These wakes are larger than the small vortex a particle would shed settling through a quiescent fluid. Following Baird's suggestion that the additional drag force induced by the shedding mechanism is proportional to the product $W \times f$ (where $W(f, A)$ is the wake volume) sufficiently high frequencies will lead to lower volume wakes or no wake at

all (if there is too little time for one to form) and retardation is weakened. Similarly, certain frequency-amplitude combinations are hypothesized to yield maximum retardation as they lead to a maximum in $W \times f$ metric [BST04]. By introducing a forced Strouhal number $Sr_f = \frac{D_p f}{U_0}$ and incorporating the influence of the flow-oscillation amplitude, captured by the ratio $\beta = \frac{A}{D_p}$, Baird correlates the magnitude of retardation to a dimensionless parameter of the form $Sr_f \beta^\alpha$ (with $\alpha = \frac{1}{3}$ serving as a fitting parameter to his experimental data for configurations in which vortex shedding occurs). Finally, Baird appeals for future work to include more detailed observations about flow patterns around particles immersed in oscillating fluids and direct measurement of the drag acting on them. The study at hand holds attempts to both.

Schöneborn [Sch75] adds to Baird's considerations of wake effects and supports the claim that the vortex shedding frequency of a falling sphere f_{nvs} can be synchronized with the frequency of the flow field f. The retarded sphere performs alternating, lateral fluctuations relative to it's falling line. If the oscillation frequency f is near the natural vortex shedding frequency f_{nvs}, resonance occurs. Schöneborn argues that drag is increased and the fall velocity decreased, because supplementary energy from the driving oscillation is transformed into wake generation. With respect to how vortex shedding influences retardation, Schöneborn argues that *"as a consequence of the shedding, asymmetries with respect to the upstream-downstream axis of the sphere appear in the wake. The wake reacting on the sphere [=shedding?] causes a fluctuation in the motion of a freely movable sphere [and in drag]. As the configuration of the wake is asymmetric, there are deflecting forces acting on the sphere, which cause a lateral motion of a freely movable sphere. The formation of a vortex is connected with an energy loss in the translational motion, consequently the actual velocity of a freely movable sphere is reduced".*

Schöneborn's study shows that vortex shedding is suppressed for increased frequencies and the lateral fluctuations stop. Increased stability of the wake during particle acceleration makes the particle depart from the solution at low Stokes number at a higher instantaneous Reynolds number than steady state results suggest [Her76]. Subsequently, retardation prediction based on a quasi-steady equation (suggested by [Hou63, Bai03, HKHK01]) underestimates the mean settling velocity. This is because the proposition that drag behaves proportionally to the velocity difference of particle and fluid $(u_{\mathrm{p}} - u_{\mathrm{f}})$, breaks when vortex shedding is suppressed and even modification of the Basset term as put forward by Ho [Ho01] does not compensate for this.

Schöneborn concludes that there are 3 regimes of particle retardation: 1) very low Sr_n, where undistorted vortex shedding allows for accurate system description by means of quasi-steady drag equation, 2) resonance: if $(f - f_{\mathrm{nvs}})$ is very small, regular lateral fluctuations around the particle falling line and increased retardation, 3) suppressed vortex shedding (equivalent to Re_p too low for vortex shedding): retardation lower than in resonance regime, but higher than in quiescent fluid. Schöneborn does not give an explanation as to what causes retardation to be higher than in a quiescent fluid or an intuition of what it's limit would be in this regime. He also does not put Baird's intuition that retardation correlates with $W \times f$ into perspective. He does, however point out that oscillation frequencies applied in experiments by Baird [BST04] and Ho [Ho01] do stay below the natural vortex shedding frequency f_{nvs}(and are therefore mostly covering regime 1). Be it due to the higher viscosity or the range of f, β tested in the work at hand, none of our simulations show any significant lateral particle motion and we cannot make a link to Schöneborn's work.

Herringe [Her76] conducted experiments in order to gain insight into phase lag, oscillation amplitude and retarded settling velocity of single particles exposed to an oscillatory flow. This is interesting, because the overall influence of Basset forces in the inertial regime could empirically be equivalent to a phase lag in fluid acceleration [OH64]. His attempt to model the drag for a wide range of configurations failed and suggested that further flow pattern analysis is required before the motion of spheres in oscillating fluids can be fully understood. An interesting idea he instantiates, but does not explore, is that β could be the determining factor on whether there is sufficient time for vorticies to develop and, that if this was so, then β also is the determining factor for the occurrence of vortex shedding for high frequency configurations.

Deng [DK90], who studied multi-particle systems in oscillatory flow as mentioned above, suggests that high particle density promotes retardation in fluids with greater viscosity and that the contribution of pressure drag, F_{dp} to the total drag, F_h increases with retardation, but does not base this assumption on measurements of the pressure fields. The former might have some dependence on the packing fraction of the multi-particle system that was studied and cannot necessarily be translated to single particle systems.

1.4 Applications

Finally, in terms of applications Mackley [Mac92] studied particle-concentration profiles along a vertically oriented column with regularly spaced orifice baffles. This contribution opens a range of industrial separation applications, as well as enhanced mixing procedures, presented in Ni's review-paper [NMH+03]. Oki [OKO+ 3, OHU+10] chose radii (D_{p1}, D_{p2}) for spheres of different density (ρ_{p1}, ρ_{p2}) such that they would have equal settling velocities $(\frac{U_{0_1}}{U_{0_2}} = 1)$ and found that the settling ratio $\frac{\overline{U_1}}{\overline{U_2}}$ (where $\overline{U}$ is the mean settling velocity of a particle in an oscillating fluid) is reduced by water oscillation. These observation makes separation by oscillation in a jig a possibly potent alternative for 'equal-settling-particles' (which are inherently equally effected by virtual gravity increase in a centrifugal separator). Pita [PC16] investigated application of oscillatory flows in a jig-apparatus to separate plastic waste. We also want to point out Spagnolie's [SS09] work which introduces a shape-changing body that adapts the surface-area exposed to a pulsating flow based on the phase of oscillation it finds itself in and demonstrates how some marine animals may be able to utilize such flows to move.

CHAPTER 2

Motivation

Understanding transport and deposition of particles in oceanic environments is critical for predicting the dispersion of materials such as nutrients, micro-plastics and hazardous waste throughout the worlds oceans. Suspended material in the ocean is often subject to oscillatory flow causing altered settling behavior. While initial research into such multi-particle systems has been conducted, the focus of this study takes a step back and focuses on the mechanism that enables single-particle retardation. Equipped with modern high resolution simulations, we find ourselves in a much better spot to find the root of this phenomenon. This is with respect to analysis of forces acting on the sphere as well as analysis of flow- and pressure-field around it. This study addresses the following questions:

1. What is the physical mechanism causing particle retardation and can asymmetries with respect to forces on and flow-structures around the particle be identified throughout a particle-oscillation?
2. What is the effect of a horizontally confined domain on particle retardation?
3. Can levitation as an extreme form of retardation be achieved in a single-particle system? If so, how does it relate to levitation in multi-particle systems?
4. Is there a dimensionless number dependent solely on material properties (ν, ρ_s) and parameters of the imposed oscillation (β, f) that captures the retardation magnitudes obtained from a wide range of parameters? If so, how does it compare to those proposed by prior contributions?

CHAPTER 3

Computational model

We use Particle Resolved Direct Numerical Simulations (PR-DNS) to investigate the retardation of a sphere in a vertically oscillating box. The Immersed Boundary Method (IBM) as proposed by Uhlmann [Uhl05] and improved by Kempe and Fröhlich [KF12] is used to model the fluid-particle interaction. The present solver has been developed and tested for accuracy by Biegert and Vowickel [BVM17, VWLFM19]. It is well equipped for grain-resolving simulations of flows over dense, granular sediment beds and lubrication modelling in this context.
The governing equations, including the modifications made to it in order to accommodate the imposed oscillations of this study, are presented in the following chapter.

3.1 Governing equations

First, we introduce the Navier-Stokes equations and the continuity equation for an incompressible Newtonian fluid for an **inertial** frame (resting coordinate system outside of the box for which the top- and bottom- boundary of the box move with the box oscillation $= u_f = -A\omega\sin(\omega t)$):

$$\frac{\partial \mathbf{u}'}{\partial t} + \nabla\cdot(\mathbf{u}'\mathbf{u}') = -\frac{1}{\rho_f}\nabla p' + \nu\nabla^2\mathbf{u}' + \mathrm{F}_{IBM} + \mathrm{F}_o \tag{3.1a}$$

$$\nabla\cdot\mathbf{u}' = 0 \tag{3.1b}$$

$$p' = p - \rho_f g, \quad \nabla p = \nabla p'$$

$$\mathrm{F}_o = \frac{\mathrm{d}\mathbf{u}_f}{\mathrm{d}t} = A\omega^2\sin(\omega t), \quad \omega = 2\pi$$

where $\mathbf{u}' = (u', v', w')^T$ is the fluid velocity-vector in Cartesian components in the inertial frame, p' the gravity-corrected pressure term, $\mathrm{F}_{\mathrm{IBM}}$ the volume force as result of the IBM and F_o the acceleration due to oscillation. Oscillation amplitude A and frequency f characterise the pulsation intensity. $\mathrm{F}_{\mathrm{IBM}}$ couples the motion of the fluid to the solid phase by acting in the vicinity of the fluid-particle interface to enforce a no-slip and no-penetration conditions on the particle surface. The Navier-Stokes and continuity equations (3.1) are integrated using a third-order low-storage

Runge-Kutta scheme in time and a second order finite difference method in space. A Fast Fourier Transform (FFT) is applied to calculate the pressure correction for continuity by means of a pressure projection method.

Subsequently, particle motion in the inertial frame is governed by the Newton-Euler equations as presented below. The hydrodynamic term $\mathbf{F}_\mathrm{h}$ couples the particle to the fluid and comprises $m_p \cdot (\mathrm{F_{IBM}} + \mathrm{F_{rigid}})$ (where $\mathrm{F_{rigid}}$ captures the transient particle motions [Bie18]). Here $I_p = \pi\rho_p D_p^5/60$ is the moment of inertia for a solid sphere and $\omega_p = (\omega_{p,x}, \omega_{p,y}, \omega_{p,z})^T$ as the angular velocity vector for the particle.

$$m_p \frac{\mathrm{d}\mathbf{u}_p'}{\mathrm{d}t} = \mathbf{F}_\mathrm{g} + \mathbf{F}_\mathrm{c} + \mathbf{F}_\mathrm{h} \tag{3.2a}$$

$$I_p \frac{\mathrm{d}\omega_p}{\mathrm{d}t} = \mathbf{M}_c + \mathbf{M}_h \tag{3.2b}$$

We wish to write the Navier-Stokes equations and the continuity equation for an in-compressible Newtonian fluid in a **non-inertial** frame (moving with the oscillatory box), because a time-depended force is much easier to implement than moving boundaies. Therefore, we need to transform the particle velocity. The non-inertial reference frame moves with $\mathbf{u}_f = (0, u_f, 0)^T$ relative to the inertial frame presented above. We can therefore write non-inertial particle velocity as $\mathbf{u}_p = \mathbf{u}_p' - \mathbf{u}_f$, where $\mathbf{u}_p' = (u_p', v_p', w_p')^T$ presents the translational velocity vector of the particle in an inertial frame. Taking the derivative of this transformation

$$\frac{\mathrm{d}\mathbf{u}_p'}{\mathrm{d}t} = \frac{\mathrm{d}\mathbf{u}_p}{\mathrm{d}t} + \frac{\mathrm{d}\mathbf{u}_f}{\mathrm{d}t}$$

and applying it to the inertial Newton equation (equation for particle motion) will yield it's non-inertial frame version.

$$m_p \frac{\mathrm{d}\mathbf{u}_p}{\mathrm{d}t} = \mathbf{F}_\mathrm{g} + \mathbf{F}_\mathrm{c} + \mathbf{F}_\mathrm{h} + (m_p - m_f)\mathrm{F}_o \tag{3.3a}$$

$$I_p \frac{\mathrm{d}\omega_p}{\mathrm{d}t} = \mathbf{M}_c + \mathbf{M}_h \tag{3.3b}$$

Here, m_p and m_f are particle mass and fluid mass (corresponding to the particle's volume). Since there are no free surfaces or density variations in the fluid, the effect of the frame acceleration is accounted for in the particle motion. As an important consequence arising from the change of the observational frame, the background acceleration of the non-inertial frame is characterized by the motion of the particle mass minus the displaced fluid mass and, hence, represents the effect of particle inertia.
The Euler-equation, however, remains unchanged, since the transformation is purely translational. The oscillatory change in the static pressure field is represented in the particle momentum equation as $\mathbf{F}_\mathrm{o}$, rather than forced on the particle from the fluid via $\mathbf{F}_\mathrm{h}$. It follows that the Lagrangian phase gets to feel the oscillation impact only by the $\mathrm{F_{IBM}}$ contribution in the Navier-Stokes equations:

$$\frac{\partial \mathbf{u}}{\partial t} + \nabla \cdot (\mathbf{u}\mathbf{u}) = -\frac{1}{\rho_f} \nabla p' + \nu \nabla^2 \mathbf{u} + \mathrm{F}_{IBM} \tag{3.4a}$$

$$\nabla \cdot \mathbf{u} = 0 \tag{3.4b}$$

where $\mathbf{u} = (u, v, w)^T$ is the fluid velocity vector in Cartesian components in the non-inertial frame.

3.2 Nondimensionalisation of the problem

We introduce characteristic scales to non-dimensionalize the governing equations where ℓ and $\mathbf{u}$ are the relevant length and velocity scales. The former is chosen as particle diameter D_p and the latter as maximal plate velocity $A\omega$. This choice yields a Reynolds number that depends both on a particle and an oscillation length scale:

$$Re = \frac{AD_p\omega}{\nu}$$

After transforming the dimensional set of variables $S = \{\ell, \mathbf{u}, t, \rho, p, m, V, F, \mathrm{F}, M, I, g, f\}$, we can write the following relations to the dimensionless counterparts $\tilde{S}$ where the tilde symbol indicates the dimensionless variable:

$$\ell = D_p\tilde{\ell}, \quad \mathbf{u} = A\omega\tilde{\mathbf{u}}, \quad t = \frac{D_p}{A}\frac{1}{\omega}\tilde{t}$$

$$\rho = \rho_f\tilde{\rho}, \quad p = \rho_f A^2\omega^2\tilde{p}, \quad m = m_f\tilde{m} = \rho_f V\tilde{m}, \quad V = D_p^3\,\tilde{V}$$

$$F = \frac{m_f A^2\omega^2}{D_p}\tilde{F}, \quad \mathrm{F} = \frac{A^2\omega^2}{D_p}\tilde{\mathrm{F}}, \quad M = m_f A^2\omega^2\tilde{M}$$

$$I = m_f\, D_p^2\tilde{I}, \quad g = \frac{A^2}{D_p}\omega^2\tilde{g}, \quad f = \frac{A}{D_p}\omega\tilde{f}$$

Finally, we obtain the dimensionless set of governing equations (Navier-Stokes, Continuity and Newton-Euler):

$$\frac{\partial \tilde{\mathbf{u}}}{\partial \tilde{t}} + \tilde{\nabla} \cdot (\tilde{\mathbf{u}}\tilde{\mathbf{u}}) = -\tilde{\nabla}\tilde{p}' + \frac{1}{Re}\tilde{\nabla}^2\tilde{\mathbf{u}} + \tilde{\mathrm{F}}_{IBM} \tag{3.4ca}$$

$$\tilde{\nabla} \cdot \tilde{\mathbf{u}} = 0 \tag{3.4cb}$$

$$\tilde{m}_p\frac{\mathrm{d}\tilde{\mathbf{u}}_p}{\mathrm{d}\tilde{t}} = \tilde{\mathbf{F}}_\mathrm{g} + \tilde{\mathbf{F}}_\mathrm{c} + \tilde{\mathbf{F}}_\mathrm{h} + \tilde{V}_p(\tilde{\rho}_p - \tilde{\rho}_f) \cdot \tilde{\mathrm{F}_o} \tag{3.4cc}$$

$$\tilde{I}_p\frac{\mathrm{d}\tilde{\omega}_p}{\mathrm{d}\tilde{t}} = \tilde{\mathbf{M}}_c \; + \; \tilde{\mathbf{M}}_h \tag{3.4cd}$$

We additionally define the Stokes number St based on fluid and particle timescales τ_f, τ_p:

$$\tau_p = \frac{D_p^2}{18\nu}(\frac{\rho_p}{\rho_f} - 1), \quad \tau_f = \frac{1}{\omega}, \quad St = \frac{\tau_p}{\tau_f} = \frac{D_p^2\omega}{18\nu}(\frac{\rho_p}{\rho_f} - 1)$$

3.3 Dimensional analysis

As laid out in the introductory section prior studies suggests that retardation is governed by the following quantities representing particle and fluid material properties as well as the oscillation of the system:

$$\omega \left[\frac{1}{s}\right], \quad A\,[m], \quad D_p\,[m], \quad \rho_f \left[\frac{kg}{m^3}\right], \quad \rho_p \left[\frac{kg}{m^3}\right], \quad \nu \left[\frac{m^2}{s}\right], \quad g \left[\frac{m}{s^2}\right]$$

We hereby assume that the geometry of a sufficiently large experimental domain, as well as particle roughness and wall properties have a negligible influence on retardation. As a well established tool in dimensional analysis the Buckingham-Π theorem [CLP82] commands that a problem governed by x quantities in y dimensions can be expressed by $x - y$ dimensionless quantities. The retardation problem counts 7 quantities comprising three dimensions (SI units) listed above. We are, therefore, in search of 4 dimensionless parameters composed of the governing physical quantities. Inspired by dimensionless terms attributed relevance to by the literature, as well as investigation of our computational data, we propose the following dimensionless set of parameters:

$$\beta = \frac{A}{D_p}, \quad \rho_s = \frac{\rho_p}{\rho_f}, \quad Re_\omega = \frac{A^2\omega}{\nu}, \quad \Gamma = \frac{gD_p^3}{\nu^2}$$

The β parameter is essential to describe oscillation geometry as it relates the two governing length scales, driving amplitude and particle diameter to another. The ratio ρ_s relates the densities of particle and fluid to another. Re_ω is a Reynolds number based on the oscillation length scale, it relates inertial to viscous forces. Γ is taken as the ratio of gravitational to viscous forces and gives information about the fluid's resistance against the particle's settling in a quiescent fluid. While the first two parameters (ρ_s, β) are frequently mentioned in literature, a multitude of parameters descriptive of oscillation intensity and fluid viscosity have been employed. Herringe [Her76] proposes as a third parameter based on the Stokes number St, $\frac{1}{f(St)} = \sqrt{\frac{\nu}{D^2\omega}}$ (which only differs from Re_ω in that the length scale applied corresponds to the particle diameter instead of the oscillation amplitude) and a fourth parameter based on the maximum fluid acceleration and gravity $\frac{A\omega^2}{g}$. He found the latter to bear the least significant correlation with retardation [Her76].
However, based on our flow-field analysis (section 4.5), we believe it is important to introduce a measure for how strongly gravity-induced settling is hindered by particle drag (Γ). The U_0-component (settling velocity in quiescent fluid) component in the Strouhal number proposed by Baird [BST04] ($Sr_f = \frac{D_p f}{U_0}$) can be interpreted in a similar fashion. We attempt to describe retardation magnitude $\frac{\overline{U}}{U_0}$, where $\overline{U}$ is the mean settling velocity of a particle settling through oscillating fluid (figure 3.2) as a function of the particle-fluid configuration and the oscillatory intensity:

$$\frac{\overline{U}}{U_0} = f(\pi_1, \pi_2, \pi_3) \text{ s.t. } \pi_1, \pi_2, \pi_3 \in \{\beta, \rho_s, Re_\omega, \Gamma\}$$

In section 4.7 we present such a relation for retardation.

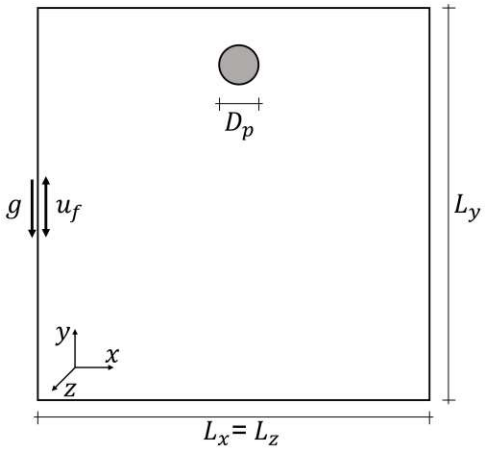

Figure 3.1: Two dimensional projection of the front view of the rectangular domain (box) spanning $L_x \times L_y \times L_z$. The non-intertial reference frame (indicated in the sketch) moves with u_f compared to a stationary inertial reference frame outside the box. Gravity acts along negative y-direction $g = (0, -9.81, 0)$. A single particle of diameter D_p is released in the center of the x, z-plane near the upper wall.

3.4 Computational set-up

3.4.1 Inspiration from experimental set-ups in literature

Experimentalists have struggled with designing a test apparatus that eliminates imperfections with respect to oscillatory motion, the particle release mechanism as well as the flow profile throughout the x, z-plane (with y being the vertical direction). Ho [Ho01] explains that his experimental setup, consisting of a fluid-filled, oscillating cylinder of height $L_z = 45cm$ and diameter $d = 9cm$, induced measurable imperfections on the sinusoidal vertical movement, as gravity caused the cylinder to lag behind the sinus during the upwards movement. From investigations into particle movement in non-uniformly oscillated fluid columns by Houghton [Hou63], Boyadzhiev [Boy20] and Deng [DK90] we know that such asymmetries can impact retardation.

Al-Taweel and Carley [ATC71] came up with a different experimental setup: Instead of measuring the settling velocity of the particle, they tuned and measured an upwards moving flow (through the oscillating test column) until it matched the particle mean settling velocity and the particle would hover at a constant height. The authors, however, had to conclude that mean settling velocities were of limited reliability because the imposed upwards moving flow led the particle to stay close to the walls. Baird [BST04] had used a similar apparatus (in that the column walls were stationary and only the fluid was pulsated). However, no superimposed upwards flow was applied and the test column maintained a larger diameter ($L_z = 305cm, d = 121cm$), such that wall effects were not identified as an issue.
The point to make is that there is a myriad of details that have had great influence on experimental studies into retardation. On top of day-to-day temperature fluctuations of the fluid, inaccuracies induced by photography-based velocity measurements, horizontal movement or rotation of the particle and alike influences might be responsible for deviations between experimental data from different groups.

3.4.2 Set-up for computational study

Moving forward, a good computational setup suffers from less imperfections, such as initial velocities and rotations upon particle release as well as asymmetries in the sinus-oscillation. Challenges arise from restraints in resolution and domain size imposed by computational limits. Herringe [Her76] used an oscillating test column with dimensions $L_z = 11.5cm \times d = 8.5cm$, where a single particle of diameter $D_p \leq \frac{d}{40}$ was released from the top of the cylinder. Tunstall and Houghton [TH09] used a similar setup with a narrower, but longer column with dimensions $L_z = 150cm \times d = 3.2cm$, where particle diameters where chosen such that $D_p \leq \frac{d}{10}$. We seek to define a setup capable of reproducing their experimental data (see section 4.2). Due to limitations imposed by the IBM, we cannot use a cylindrical geometry, and instead use rectangular prisms. The computational domain employed in this study spans $L_x \times L_y^{(\mathrm{I,II})} \times L_z = 10D_p \times \{40D_p^{(\mathrm{I})}, 70D_p^{(\mathrm{II})}\} \times 10D_p$, where the horizontal dimensions $L_x = L_z$ arise from a convergence study laid out in section 4.1. The first domain height, $L_y^{(\mathrm{I})}$ is taken from a prior study on the settling of sediment using the same code [VBLFM19] and in this study is employed for simulation configurations with low quiescent settling velocities U_0 or low oscillation amplitudes A. In cases with large oscillation amplitudes ($A_{max} \geq 30D_p$), a taller domain, $L_y^{(\mathrm{II})}$, is required to avoid collisions between the suspended particle and the bottom boundary. We define the domains Θ_{10}, Θ_6:

$$\Theta_{10} = 10D_p \times \{40D_p^{(\mathrm{I})}, 70D_p^{(\mathrm{II})}\} \times 10D_p$$
$$\Theta_6 = 6D_p \times \{40D_p^{(\mathrm{I})}, 70D_p^{(\mathrm{II})}\} \times 6D_p$$

where Θ_6 is tested in order to the influence a horizontally confined domain.
We assume the vertical span L_y has no influence on retardation magnitude $\frac{\overline{U}}{U_0}$, therefore it is not declared if $L_y^{(\mathrm{I})}$ or $L_y^{(\mathrm{II})}$ has been used in a specific simulation. No-slip conditions are imposed on the vertical and horizontal walls in order to best match the experimental setup. Finally, in accordance with a convergence study (section 4.1) a cubic mesh of grid spacing $h = \frac{D_p}{20}$ is used to discretize the domain.

3.5 Retardation measurement

Retardation magnitude $\frac{\overline{U}}{U_0}$ is measured by relating the mean settling velocity of a particle settling through oscillating fluid $\overline{U}$ to the settling velocity U_0 of the same particle through quiescent fluid. In order to define these velocity quantities two simulations O, Q where O corresponds to the oscillatory situation and Q to the quiescent situation are conducted. O and Q are similar with respect to material properties (ρ_s, ν), but differ in terms of oscillatory motion (ω, β) such that $\beta_Q = \omega_Q = 0$ (thereby $Re_{\omega Q} = 0$).

Figure 3.2 illustrates typical trajectories for simulation O and Q. The trajectory for the oscillatory data has to be filtered by the oscillation frequency f_O in order to obtain the particle's mean settling trajectory corresponding to $\overline{U}$. This can be done by employing an FFT or simpler: by extracting one data-point at the same relative position in time from each oscillation. In

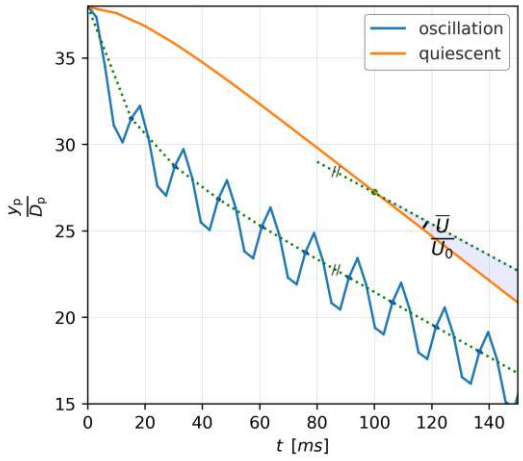

Figure 3.2: Retardation $\frac{\overline{U}}{U_0}$ illustrated in visual terms. Particle trajectory in quiescent fluid (orange) with settling velocity U_0 and mean particle trajectory in oscillatory case (green) with mean settling velocity $\overline{U}$ in quasi-steady state yield an angle indirectly proportionate to retardation magnitude.

this manner one obtains a set of data points $X = \{y_0, y_T, y_{2*T}, .., y_{i*T}\}$ which are separated by one period $T = f^{-1}$ in time. Both Schöneborn [Sch75] and Al-Taweel [ATC71] record that the period of the induced oscillation in the particle matches that of the fluid, therefore mean settling trajectories are comparable throughout an oscillation-parameter $(f, beta)$-sweep.
$\overline{U}$ is the gradient of the set X with respect to time, when only the partition of X for which the terminal velocity (terminal mean velocity in simulation O) has been reached is considered. In prior experiment procedures disregard of non-terminal velocity data was ensured by not considering the particle trajectory for the first vertical $25cm$ from the release point [TH09].

CHAPTER 4

Numerical investigation

4.1 Convergence study

The computational set-up for the study at hand is described in section 3.4. Here we lay out the justification for choosing domain Θ_{10} and a cubic mesh of grid spacing $h = \frac{D_p}{20}$. The primary objectives of this convergence sutdy are to 1) determine $L_x = L_z$ such that wall effects induce only a small error on settling velocity measurements and 2) determine the resolution h such that small flow details are captured to a sufficient degree.

4.1.1 Domain width

Convergence with regards to the horizontal domain span is checked for two combinations of material and oscillation parameters. The specific characteristics were taken from Herringe's experimental documentation [Her76] and correspond to configuration ID=1,3 with $Re_1 = 47, Re_3 = 283$ and $\rho_{s1} = \rho_{s3} = 2.96$ (table 5.2). Simulations grid spacing $h = 20$ for 6 different horizontal domain sizes were conducted in quiescent and oscillating fluid. The relative error in mean settling velocity U based on the mean settling velocity of the largest domain-size tested computed accordingly (see figure 4.1).

The domain's horizontal span influences the (mean) settling velocity, more so in oscillatory ($\overline{U}$) than in quiescent fluid (U_0). Velocities in a confined space tend to underestimate those observed in a system characterized by $L_x = L_z = \infty$. Lapple [Lap56] suggests that the proximity of a rigid cylindrical wall can noticeably increase the drag on a sphere falling in water when the particle diameter is ten times smaller compared to that of the test-tube ($\frac{L_{x,z}}{D_p} < 10$) and more specifically that a diameter-domain-ratio of ($\frac{L_x}{D_p} = 7$) can lead to an error of 1%. Our data for the lower-viscosity-situation ($ID = 3, \nu_3 = 1e^{-6}\frac{kgm^2}{s}$) suggests a comparable relative error err_{rel} of 2% in the quiescent and 5% in the oscillated situation for domain Θ_6 ($\frac{L_{x,z}}{D_p} = 6$). However, in the more viscous situation ($ID = 1, \nu_1 = 2e^{-5}\frac{kgm^2}{s}$) err_{rel} is 12% in in the quiescent settling case and 19% in the oscillated case for Θ_6. We believe the increased wall influence in a set-up with a more viscous fluid is due to more 'rigid' coupling between particle and wall compared to a

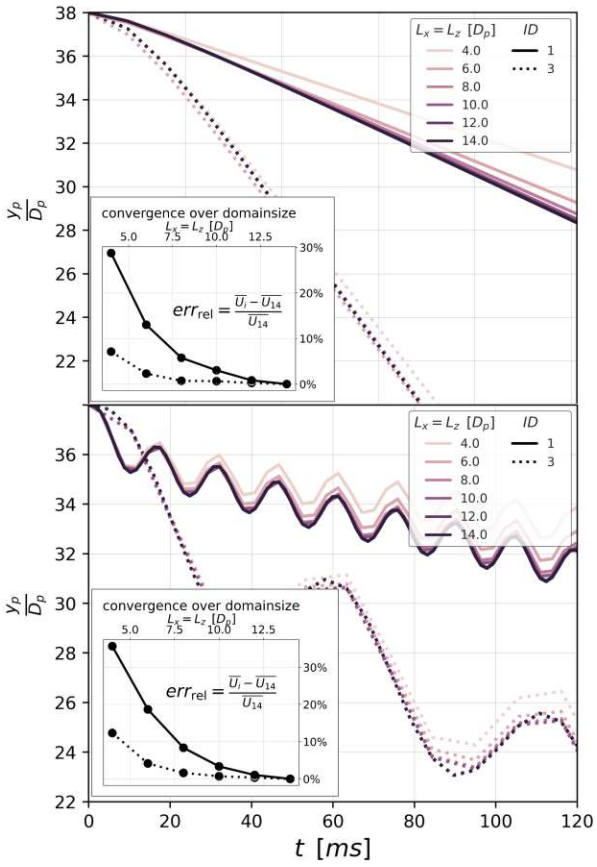

Figure 4.1: Particle trajectories in quiescent (*top*) and oscillating fluid (*bottom*) for material configurations ID=1,3 over time for domain spans L_x=L_z=$\{4D_p, 6D_p, 8D_p, 10D_p, 12D_p, 14D_p\}$. *(insets)* Relative error err_{rel} based on the mean settling velocity $\overline{U_{0_{14}}}$ measured for the largest horizontal span $L_x = L_z = 14D_p$ tested.

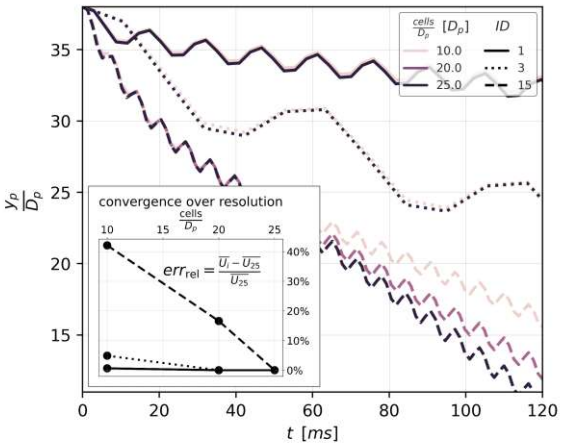

Figure 4.2: Particle trajectories in oscillating fluid for retardation configurations ID=1,3,15 over time for resolutions $h = \{10, 20, 25\}$. *(inset)* Relative error err_{rel} based on the mean settling velocity $\overline{U_{25}}$ measured for the most resolved simulation $h = 25$.

fluid characterized by less inner friction.

The relative error err_{rel} converges for growing horizontal spans. It is $< 3\%$ and $< 4\%$ for the quiescent and oscillatory case, respectively, in the Θ_{10} domain (for $\nu_1 = 2e^{-5}\frac{kgm^2}{s}$). Since both, the mean settling velocity from the quiescent U_0 and oscillatory flow situation $\overline{U_0}$ in a confined horizontal space underestimate their theoretical counterparts for $L_x = L_z = \infty$, the ratio counterbalances some of the error in the retardation $\frac{\overline{U}}{U_0}$.

4.1.2 Resolution

Simulations for configurations $ID = 1, 3$ are conducted for different resolutions $h = 10, 20, 25$ with domain Θ_6. The relative resolution error remains low for configurations $ID = 1, 3$. An investigation into the most inertia-dominated configuration documented by Herringe (ID=15,

$\frac{\overline{U}}{U_0}_{\text{exp}}$ [-]	ρ_s [-]	ν [$\frac{kgm^2}{s}$]	β [-]	f [Hz]
0.71-1.0	2.96-11.4	$2.5e^{-7} - 4.0e^{-5}$	1.3-6.0	20-160
0.00*-0.88	2.96,11.4	$2.6e^{-5}, 2.2e^{-5}$	10-30	30-125

Table 4.1: parameter span original Herringe Data-Set (*top*, table 5.2, 5.3 upper part) and Herringe Data-Set extension (*bottom*, 5.2, 5.3 lower part)

$Re_{15} > 5e^3, \nu_{15} = 2.5e^{-7}\frac{kgm^2}{s}$) shows a drastically increased error metric. As a precaution all simulations conducted (section 4.3) will be designed such that $Re_p < 1e^3$ by relying on viscosity in proximity of ν_1. As previously used and recommended by Biegert [Bie18] and Vonwickel [VWLFM19] resolution of $h = \frac{D_p}{20}$ is employed.

4.2 Validation of numerical results

Herringe's work [Her76] records 29 parameter configurations, 20 of which were reproduced numerically in this study. This is to ensure the computational model described in section 3.4 and used for all further investigation is a valid approximation to the physical situation. (The remaining configurations are characterized by combinations of very low viscosity ν and high density ratio ρ_s, such that the limited vertical dimension of our simulation domain ($L_y = 70D_p$) causes the particle to collide with the lower boundary before reaching a terminal state.) Experimentally observed retardation magnitudes $\frac{\overline{U}}{U_0}$ span 0.72-1.00, the system according configurations span a wide range of parameters (table 4.1). The median, average, minimum and maximum relative errors obtained by simulation compared to the experimental results $err_{\text{num}} = \frac{|\frac{\overline{U}}{U_0}_{\text{exp}} - \frac{\overline{U}}{U_0}_{\text{num}}|}{\frac{\overline{U}}{U_0}_{\text{exp}}}$ are 2.5%, 3.5%, 0.6% and 9.1%. Full information on all validation runs and their experimental counterparts is declared in table 5.2.

4.3 Data-set extension

Based on the material configurations investigated by Herringe (table 5.2) we extend the parameter space with regards to oscillation intensity (β, f). That is by adopting the material configurations ID=0,26 (which proved low in error between experiment and simulation). Both are characterized by viscosity high enough to maintain Re well below $1e^3$, as well as to allow the particle to reach quasi-steady settling before collision with the lower boundary. Viscosities $\nu_0 = 2.2e^{-5}, \nu_{26} = 2.6e^{-5}$ are in close proximity to ν_3 for which convergence was tested in section 4.1. Particle densities resemble sediment and metal in water $\rho_{s0} = 2.96, \rho_{s26} = 11.4$. β values of up to 30 and f values of up to $125Hz$ were tested, respectively.
Particle Reynolds numbers Re_p tend to be much lower for ρ_{s0} than ρ_{s26} configurations (< 150, < 500 respectively). This is, because high density ratios translate large oscillation amplitude-ratios β into large particle-amplitudes (non-inertial frame) much more effectively than low density-ratios. Observed retardation magnitudes span 0.00-0.88, where levitation $\frac{\overline{U}}{U_0} = 0.00$ levitation was observed for ID=83. However, this is the culmination of a sweep of configurations for which particle trajectories do not satisfy quasi-steady settling conditions. They are discussed in detail in section 4.6, but ignored here. Configuration details and dimensionless numbers on all tested configurations can be found in tables 5.3, 5.2.

4.3.1 Unconfined domain Θ_{10}

Stronger retarding effects than reported by prior studies were observed ($\frac{\overline{U}}{U_0} = 0.07$ for ID=77 being the minimum). To put this into perspective, the lower bound observed in prior experimental data (obtained from a similar one-particle system set-up) was 0.48 by Ho (metal sphere in water-glycerol mixture and large $\beta = 40$ at much lower $f = 7$Hz)). ID=77 is characterized by comparable $\beta = 30$, but much higher $f = 65$Hz, fluid viscosity larger by two magnitudes and a density ratio double that of Ho's experiment. However, with the ratio of plate to particle oscillation amplitude to vertical domain span being $\frac{15}{70} = 0.21$ (meaning the particle transitions through almost half of the vertical domain configuration ID=77 (and all other configurations with $\beta = 30$) are potentially not free of influence from the limited vertical domain span. Taking the $\beta = 25, 30$ configurations out of configuration, the strongest retardation effect was for ID=65 with $\frac{\overline{U}}{U_0} = 0.4$.

Retardation generally increases with the amplitude-ratio β (equivalent to A as all simulations are parameterized such that the particle diameter $D_p = 1$mm). The same does not necessarily hold true for oscillation frequency f. While it is obvious that the initial introduction of an oscillation in the flow (going from $f = 0$ to $f > 0$) does benefit retardation (as in: it enables the phenomenon in the first place), frequency increments further up along the spectrum do not necessarily cause an increase in retardation. f-sweeps I,II (table 4.2) demonstrate that retardation hits a limit for ceteris-paribus frequency increments and even passes a minimum (f-sweep I). Experimental data supports the observation of a retardation-minimum [TH09], [BST04]. An explanation attempt for the occurrence of this minimum was made by Baird [BST04] and discussed in section 1.3 at length. Tunstall [TH09] mentions that the minimum becomes less prominent as D_p is decreased. A ceteris-paribus diameter decrease in experiment is equal to a ceteri-paribus increase in β in our simulation setup (if the ratio of particle size to domain size is ignored). f-sweep II and III are a ceteris paribus β increase, the increased oscillation amplitude A in sweep III seems to enable further retardation, which makes the sweep unsuitable to assess Tunstall's claim. No other with a smaller toggle of β is available.

4.3.2 Confined domain Θ_6

Comparison between the results from the Θ_{10} and Θ_6 domain (table 4.2) confirms that a particle in the confined space is generally retarded more strongly. The difference in retardation magnitude is in accordance with the error estimate presented in section 4.1 (convergence study). At the same time, particle velocities u_p (represented by Re_p) are barely affected by confinement. Ceteri-paribus f- and β-sweeps in the confined domain show consistent convergence of retardation and no local minima. Picking up on Schöneborn's [Sch75] resonance-theory (described in section 1.3) we assume that wake-generation around the particle in a system with altered domain-size is qualitatively changed. Section 4.5 gives a description of these changes.

				Θ_{10}		Θ_6	
ID	β [-]	f [Hz]	Re [-]	$\frac{\overline{U}}{U_0}$ [-]	Re_p [-]	$\frac{\overline{U}}{U_0}$ [-]	Re_p [-]
β sweep I, $\rho_s = 11.4$							
26	2.6	**65.9**	41	0.79	34	0.72	34
64	15.0	**65.0**	235	0.59	161	0.40	160
65	20.0	**65.0**	313	0.40	208	0.26	206
76	25.0	**65.0**	392	0.28	267	0.24	266
77	30.0	**65.0**	470	0.07	316	0.04	314
β sweep II, $\rho_s = 2.96$							
33	10.0	**60.0**	172	0.88	53	0.59	86
41	20.0	**60.0**	343	0.83	93	0.48	92
68	25.0	**60.0**	361	0.71	87	0.38	87
69	30.0	**60.0**	434	0.63	99	0.39	99
f sweep I, $\rho_s = 2.96$							
39	**20.0**	20.0	114	0.75	22	0.73	22
40	**20.0**	40.0	229	0.72	55	0.50	55
41	**20.0**	60.0	343	0.83	92	0.48	92
70	/	/	/	0.00	/	0.42	98
71	**20.0**	85.0	410	0.79	114	0.42	114
f sweep II, $\rho_s = 11.4$							
63	**10.0**	30.0	72	0.59	49	0.52	49
100	**10.0**	45.0	108	0.59	77	0.46	77
96	**10.0**	60.0	145	0.65	104	0.45	103
61	**10.0**	105.0	253	0.60	184	0.44	183
f sweep III, $\rho_s = 11.4$							
97	**20.0**	30.0	144	0.59	87	0.38	86
101	**20.0**	45.0	216	0.59	139	0.34	138
98	**20.0**	60.0	289	0.45	190	0.33	190
65	**20.0**	65.0	313	0.40	208	0.26	206

Table 4.2: Retardation over ceteris paribus β- and f-sweep for domains Θ_{10}, Θ_6 (full information in table 5.2 and table 5.3 lower part)

4.4 Investigation into particle drag

4.4.1 Metrics for drag contribution

Consider the particle force balance over one oscillation period T in a state in which the terminal mean particle velocity has been reached (quasi-steady settling) and no collision occurs. In this terminal state an equilibrium of imposed forces ($\tilde{\mathbf{F}}_\mathrm{g}, \tilde{\mathbf{F}}_\mathrm{e}$) and the hydro-static force $\tilde{\mathbf{F}}_\mathrm{h}$ is required in order to fulfill the zero-'mean'-acceleration.

$$\tilde{m}_p \underbrace{\int_T \frac{\mathrm{d}\tilde{\mathbf{u}}_p}{\mathrm{d}\tilde{t}}\, dt}_{0} = \int_T \tilde{\mathbf{F}}_\mathrm{g} - \tilde{\mathbf{F}}_\mathrm{h} + \underbrace{\tilde{V}_p(\tilde{\rho}_p - \tilde{\rho}_f)\cdot \tilde{\mathrm{F}_o}}_{\tilde{\mathbf{F}}_\mathrm{e}}\, dt \tag{3.4a}$$

Considering that the oscillation induced external force $\tilde{\mathbf{F}}_\mathrm{e}$ is a perfectly harmonic function without asymmetry over time, it's integral over the period T is zero and we obtain the following relation between work done by gravity and hydro-static effects over an oscillation period:

$$\int_T \tilde{\mathbf{F}}_\mathrm{g}\, dt = \int_T \tilde{\mathbf{F}}_\mathrm{h}\, dt - \underbrace{\int_T \tilde{\mathbf{F}}_\mathrm{e}\, dt}_{0} \tag{3.4b}$$

In order for $\int_T \tilde{\mathbf{F}}_\mathrm{h}\, dt > 0$ (net lift) to hold the hydro-static force has to be asymmetric over the course of a period, that is: it's magnitude has to be larger throughout the particles downwards movement. In order to compare different parameter configurations and draw conclusions with respect to the magnitude of retardation, we need to dissect the hydro-static force term (since the period-integral over the entire term has to match gravity regardless of retardation magnitude). We propose to split the hydro-static term $\tilde{\mathbf{F}_\mathrm{h}}$ into a component $\tilde{\mathbf{F}_\mathrm{dp}}$ that is due to the difference in pressure between the particle's tail and tip (vertically axis) and a component $\tilde{\mathbf{F}_\mathrm{dv}}$ comprising viscous drag effects. Applying the partition to equation (4.4.1) yields:

$$\int_T \tilde{\mathbf{F}}_\mathrm{g}\, dt = \int_T \tilde{\mathbf{F}}_\mathrm{dp}\, dt + \int_T \tilde{\mathbf{F}}_\mathrm{dv}\, dt \tag{3.4c}$$

$\tilde{\mathbf{F}_\mathrm{dp}}$ is extracted from simulation data on $\tilde{\mathbf{F}_\mathrm{h}}$ by interpolation and consequent integration of the pressure field apparent on the sphere surface. The viscous contribution $\tilde{\mathbf{F}_\mathrm{dv}}$ can be determined by subtraction. The integral $\int_T \tilde{\mathbf{F}}_\mathrm{dp}\, dt$ can be interpreted as the reduction in particle velocity caused by the pressure contribution over one quasi-steady period.

We are interested in the contributions to the drag asymmetry $C_\mathrm{dp}, C_\mathrm{dv}$ and the phase shifts ϕ_h, ϕ_y between the reactionary force $\tilde{\mathbf{F}_\mathrm{h}}$ and the particle location y_p to the external oscillation force $\tilde{\mathbf{F}}_\mathrm{e}$ extorting particle motion.

$$C_{dp} = \int_T \frac{\tilde{\mathbf{F}}_\mathrm{dp}}{\tilde{\mathbf{F}}_\mathrm{g}} \qquad C_{dv} = \int_T \frac{\tilde{\mathbf{F}}_\mathrm{dv}}{\tilde{\mathbf{F}}_\mathrm{g}} = 1 - C_{dp}$$

$$\phi_h = \phi(\tilde{\mathbf{F}_\mathrm{h}}, \tilde{\mathbf{F}_\mathrm{e}}) \qquad \phi_y = \phi(y_p, \tilde{\mathbf{F}_\mathrm{e}})$$

As illustrated in fig 4.3 there is a 'delay' between $\mathbf{F}_\mathrm{dp}$ and $\mathbf{F}_\mathrm{dv}$ for more retarded particle settling trajectories. It becomes visibly shortly before the particle changes it's direction ($u_p = 0$), to be

precise, when the reactionary hydro-static force $F_h = 0$. We define the 'quasi-phase-shift' as quantification for this 'delay':

$$\phi_{vp} = \frac{\Delta(t_{A=0.75})}{T} \cdot 360°$$

where T is the oscillation period length and $\Delta(t_{A=0.75})$ is the delay of $\tilde{\mathbf{F}}_{\mathrm{dp}}$ compared to $\tilde{\mathbf{F}}_{\mathrm{dv}}$ hitting 75% of their maximum respective amplitude. This parameter essentially represents the delay of pressure force versus viscous drag.

4.4.2 Analysis of drag contribution

Retardation configurations characterized by material configuration $\rho_{s26} = 11.4, \nu_{26} = 2.6e^{-5}$ (only ID=103 has $\rho_{s0} = 2.96$) have been investigated with regards to drag contributions. These configurations yield a wide range of retardation magnitudes (0.45-0.84 for the Θ_{10} domain) in quasi-steady particle settling. Therefore, a single period N_T from the quasi-steady-state part of the particle settling trajectory can be observed representative of the whole trajectory. In the hope to extract the physical reason for the retardation increase in confined domains, the study is conducted for the two domain-configurations introduced in earlier sections (domains Θ_6 and Θ_{10}). Table 4.3 holds all configuration details and resulting quantities.

Figure 4.3 illustrates the particles reaction to the flow oscillation for a number of configurations that diverge greatly in terms of retardation (and other than ID=103 only differ by (β)). The plots illustrate a few key observations that we will try to quantify numerically (table 4.3):

1. The strength of the reactionary force F_h and it's contributions due to pressure difference and viscous drag (F_{dp}, F_{dv}) vary with β and the contribution of the former compared to the latter increases with the retardation effect.

2. The shift between the peak of the contributions due to pressure difference and viscous drag (F_{dp}, F_{dv}) increases with oscillatory intensity and the 'delay' ϕ_{vp} in the pressure contribution F_{dp} becomes more eminent.

3. The phase-lag between reactionary force F_h and oscillation force F_e increases with oscillatory intensity, not necessarily with retardation.

4. The phase-lag between reactionary force F_h and particle trajectory y_p is barely affected by changes in the oscillation amplitude β and frequency f.

These initial observations suggest that the pressure contribution to the net-lift C_{dp}, as well as the pseudo-phase-shift ϕ_{vp} as quantitative measure for the 'delay' of F_{dp} hold the most information. The former is in line with Deng's analysis [DK90] that suggests the pressure gradient contributes stronger to retardation than the effect of viscous drag. We can also confirm Carsten's hot-wire anemometer-study [Car10] indicating that the velocity-difference in front of and behind the oscillating sphere becomes more pronounced with increased β. This must cause greater pressure differences, hence the pressure contribution becomes more and more important as oscillatory intensity increases. We are interested in linking these physical phenomena to retardation magnitude $\frac{\overline{U}}{U_0}$.

Figure 4.4 visualizes the data held in table 4.3 and plots retardation magnitude over the parameters ϕ_{vp} and C_{dp}. Normalization by both oscillation parameters ($\frac{C_{dp}}{\beta f}, \frac{\phi_{vp}}{\beta f}$) leads to the correlation with similar slopes. Both the 'delay' in the pressure force (ϕ_{vp}) and the pressure contribution to the net-lift (C_{dp}) become more and more prominent for configurations with high retardation. The upper left plot in figure 4.4 demonstrates that in order to achieve a similar retardation effect in a larger domain (at constant f), the pressure force needs to contribute more to the net-lifting force. Larger amplitudes A are necessary. The correlation between the pressure force contribution C_{dp} and the severity of the pressure force-'delay' (ϕ_{vp}) indicates that the latter boosts the asymmetry in pressure force (in upwards- versus downwards movement).

ID	ρ_s[-]	N_T	$\frac{\overline{U}}{U_0}$ [-]	β [-]	f [Hz]	ϕ_{vp}[°]	C_{dp}[-]	ϕ_h[°]	ϕ_y[°]
Θ_{10}									
99	11.4	6	0.84	2.6	30.0	7.49	0.39	129	208
102	11.4	9	0.80	2.6	45.0	9.77	0.42	126	201
26	11.4	14	0.79	2.6	65.9	12.15	0.47	126	197
63	11.4	6	0.59	10.0	30.0	14.63	0.50	129	208
100	11.4	9	0.59	10.0	45.0	21.64	0.63	129	205
96	11.4	9	0.65	10.0	60.0	28.7	0.75	129	201
97	11.4	6	0.46	20.0	30.0	18.29	0.59	136	212
101	11.4	9	0.47	20.0	45.0	27.11	0.76	133	208
98	11.4	9	0.45	20.0	60.0	36.05	0.92	129	205
103	2.9	9	0.78	20.0	60.0	22.27	0.48	158	215
Θ_6									
99	11.4	6	0.81	2.6	30.0	7.42	0.39	129	208
102	11.4	9	0.71	2.6	45.0	9.56	0.42	125	201
26	11.4	14	0.72	2.6	65.9	12.11	0.47	126	197
63	11.4	6	0.51	10.0	30.0	13.87	0.50	129	208
100	11.4	9	0.46	10.0	45.0	21.2	0.58	129	205
96	11.4	9	0.44	10.0	60.0	28.55	0.69	126	201
97	11.4	6	0.38	20.0	30.0	18.14	0.60	136	212
101	11.4	9	0.35	20.0	45.0	26.8	0.70	133	208
98	11.4	9	0.33	20.0	60.0	35.86	0.72	129	205
103	2.9	9	0.44	20.0	60.0	22.33	0.62	158	215

Table 4.3: C_{dp} and $\phi_h, \phi_y, \phi_{vp}$ as well as the main system parameters for the force-contribution-analysis configurations. The configurations test the β-f-parameter grid defined by $\beta = \{2.6, 10, 20\} \times f = \{30, 45, 60\}$

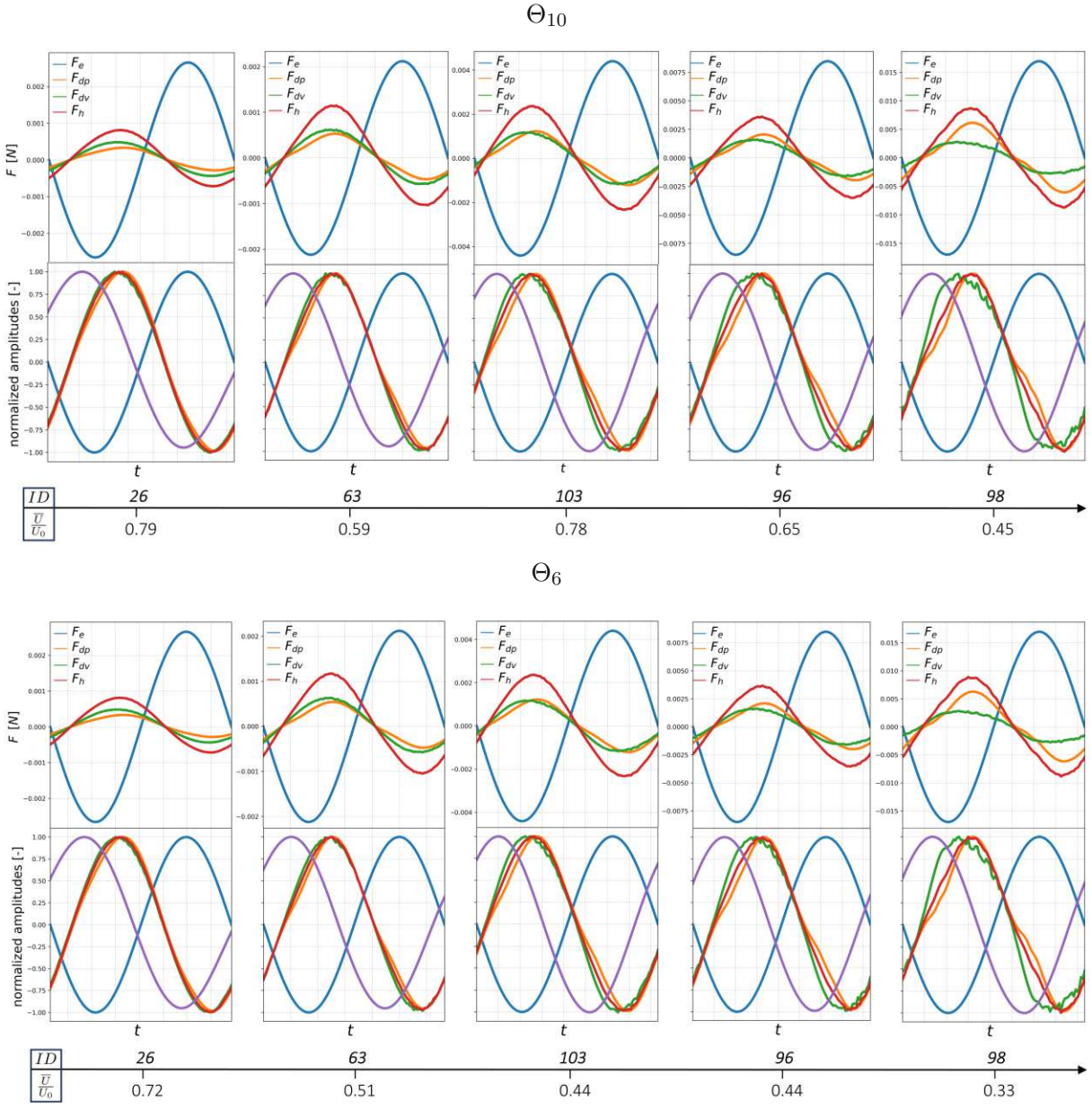

Figure 4.3: *tops*: The contribution of forces acting on the particle over an oscillation period, where $\mathbf{F}_\mathrm{h}$ $(= \mathbf{F}_\mathrm{dp}, \mathbf{F}_\mathrm{dv})$ are reactionary to $\mathbf{F}_\mathrm{e} + \mathbf{F}_\mathrm{g}$ (the latter is constant negative and not illustrated in the figure). *bottoms*: The same force contributions and the particle trajectory y_p normalized by their respective amplitude maxima.

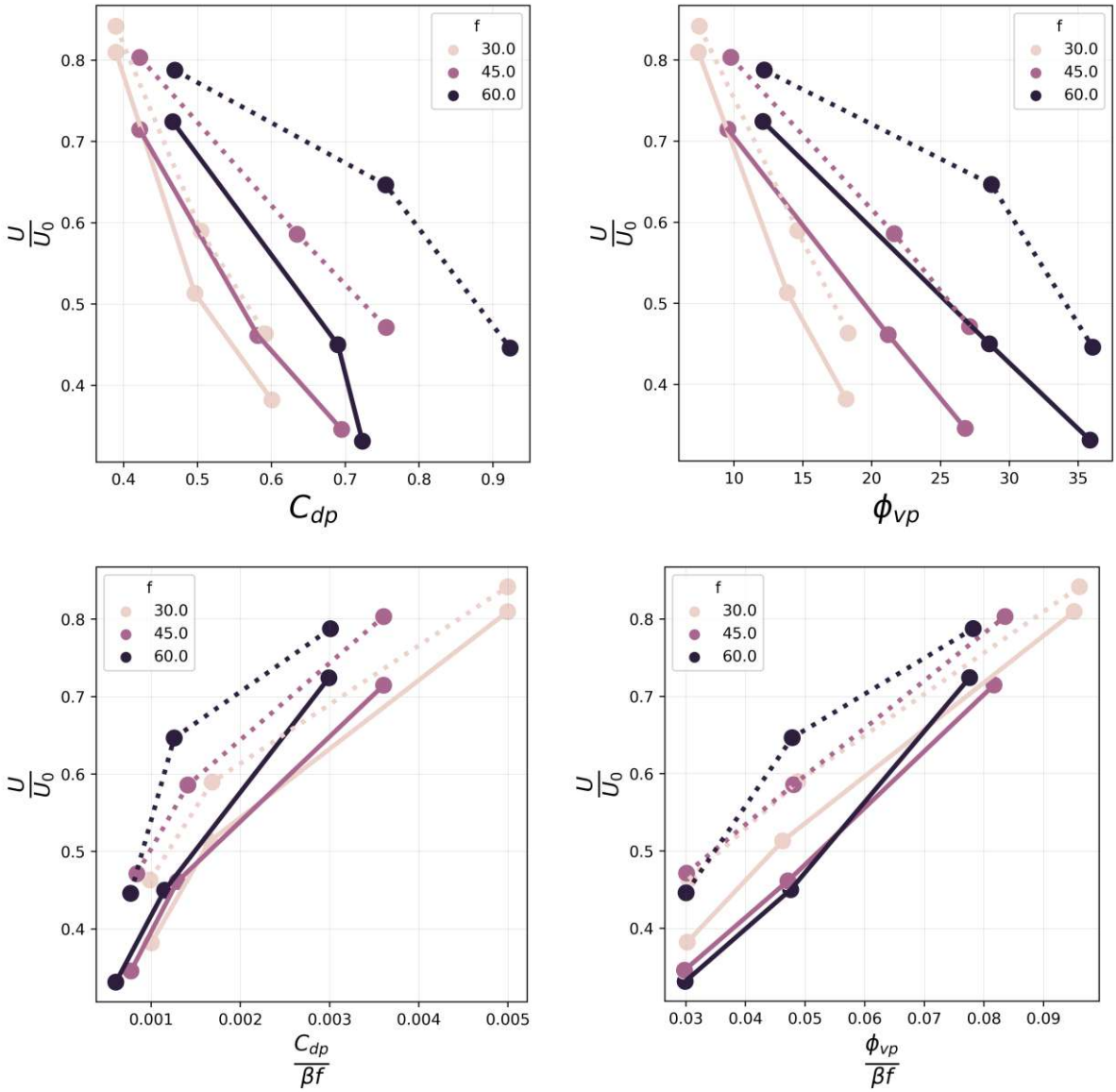

Figure 4.4: Retardation $\frac{\overline{U}}{U_0}$ over C_{dp} (*left*) and ϕ_{vp} (*right*) for different normalizations based on table 4.3 where dotted lines indicate data from domain Θ_{10} and full lines from domain Θ_6

4.5 Flow field analysis

The following is a qualitative description of differences in flow patterns caused by changes in β, f, ρ_s and the domain-size $L_x = L_z$. It is also an attempt to link the pressure force-'delay' ϕ_{vp} described in the prior section to characteristics of the flow-field. For this purpose flow patterns of the configurations ID=26,96,98 (const. f) and ID=63,96 (const. A) were analyzed over a half-period of the particle oscillation (illustrated in figures 4.5-4.12). Additionally, changes caused by an alteration in domain-size (Θ_{10} (L_x=L_z=$10D_p$) to Θ_6 (L_x=L_z=$6D_p$)) occurring in the flow-field were analyzed for configurations ID=26,98,96,103.

4.5.1 Influence of amplitude

Figures 4.5,4.7 and 4.8 illustrate snapshots of both velocity- and pressure field over a half-period of the particle oscillation in quasi-steady state in the configurations ID=26,96,98 with constant $f = 60$, but over different amplitude-ratios $\beta = 2.6, 10, 20$ for the Θ_6 domain.

Focusing on the most retarded configuration 98 ($\beta = 20$, $\frac{\overline{U}}{U_0} = 0.33$) first, the flow-profile during the particle's upwards-movement shows a separated flow structure ahead of the particle ('heading vortex'). The particle's trailing vortex absorbs the heading vortex when the system transitions from the regime in which the particle is driving the fluid, to being driven (much like a ship will be affected from it's trailing flow if the propeller-direction is inverted when in cruise - 'inverted propeller transition'). The upwards streaming fluid causes increased pressure on the particle's tail, the reactionary force goes to zero $F_h = 0$ (following figure 4.4), while the particle is still in upwards-movement. The flow field will now be dominated by a single, vertically far stretching ('global') vortex until the particle's change of direction generates a wake that causes separation of the global vortex. During the 'single-vortex'-phase the pressure difference between head and tail remains low. The flow field a half-period after the initial frame $t_5 = t_5 + T/2$ is qualitatively similar.

The situation described for the least retarded configuration 26 ($\beta = 2.6$, $\frac{\overline{U}}{U_0} = 0.72$) differs greatly. The particle's upwards-moving phase is characterized by separated vertices which (in contrast to the ID=98 situation) sustain throughout 'inverted propeller transition'. During the downwards-movement of the particle the flow-field simplifies and is eventually reduced to a single global vortex. This vortex remains intact until the particle transitions into upwards-movement again. Throughout the vast part of the downwards-movement the flow-field is very different compared to upwards-movement equivalent. This is in such fashion that the particle meets more resistance (by a heading vortex) during the upwards-movement compared to the downwards-movement.

The flow-field of the configuration 96 ($\beta = 10$, $\frac{\overline{U}}{U_0} = 0.44$) differs from ID=98 through the smaller expansion of the global vortex. This difference causes the heading vortex (of the downwards-movement) to carry less energy and dissipate much earlier (it remains intact much longer than in ID=26, respectively).

We hypothesize that the flow field asymmetry occurs if gravity is dominant compared to the oscillation-induced effects. As a result of 'global vortex'-phase during the downwards movement and the lower-pressure difference induced by it the particle is facing qualitatively lower resistance compared to the upwards movement (dominated by separated vertices). It appears that higher β

breaks gravity-dominance and imposes flow-field-symmetry for longer stretches of the downwards- compared to upwards movement.

4.5.2 Influence of frequency

Figures 4.11,4.12 illustrate snapshots of both velocity- and pressure field over a half-period of the particle oscillation in the configurations ID=63,96 with constant $\beta = 10$, but different frequencies $f = 30, 60$ (we base this analysis on the Θ_{10} results). The 96 ($f = 60$, $\frac{\overline{U}}{U_0} = 0.65$)-configuration was described in the section above, it remains to compare it qualitatively to 63 ($f = 30$, $\frac{\overline{U}}{U_0} = 0.59$).

The clue to the difference of the ID=63 flow-field compared to the ID=96-situation is lower-energy in the system (as the oscillation causes much lower acceleration forces - see figure 4.3). Other than a less pronounced pressure field, this causes the heading vortex to dissipate much earlier in the upwards movement than in ID=96 (the vortex is long gone when the first frame is taken). The same is even more true for the downwards-movement (frame t_0) and the particle is subject to suspended downwards-movement (with an intact heading vortex) much shorter.

4.5.3 Influence of confined space

Figures 4.9,4.12, 4.13 and 4.10 illustrate snapshots of both velocity- and pressure field over a half-period of the particle oscillation in the configurations ID=26,96,98,103 for the Θ_{10} domain. The differences in retardation compared to the Θ_6 simulations $\frac{\overline{U}}{U_0}_6 - \frac{\overline{U}}{U_0}_{10} = \{0.07, 0.21, 0.12, 0.25\}$ are large. Figure 4.3 and figure 4.4 illustrate that the parameters ϕ_{vp} and C_{dp} (measuring delay of pressure force versus viscous drag and the former's contribution to the net-lift) are slightly shifted. At the same time, this shift of particles-force-magnitude eminent over a period is merely detectable visually (figure 4.3).

The comparison of configuration pairs ID=26,103,96,98 demonstrates greater asymmetry between up- and downwards-moving phase in the larger domain Θ_{10}. The heading-vortex the particle settles against in the downwards-phase collapses earlier in the Θ_{10}-domain and leaves the downwards-movement with a longer time-span during which it differs from the upwards-movement (a half-period $\frac{T}{2}$ ahead). Confined domain imposes more symmetry on up- versus downwards-movement.
An additional qualitative flow-field difference in the configuration-pair 98 ($\frac{\overline{U}}{U_0}_6 = 0.33$, $\frac{\overline{U}}{U_0}_{10} = 0.45$) is that where the small-domain flow comprises only a single global vortex during the 'inverted propeller transition' the large domain holds a more complex situation. This unbroken vortex separation potentially increases resistance on the particle during the upwards-movement-phase of the 'inverted propeller transition'. The broader horizontal span causes a less stretched heading-vortex that is dissolved easier.

It appears that decreased domain-width leads to reduction of the asymmetry found between the particle's up- and downwards-movement. The effect can be quantified by timing the dissipation of the heading vortex during the downwards- and the upwards-movement (since only a global vortex remains after this event). We obtain an asymmetry-metric a_{ud} (table 4.4) that indicates for which partition of the downwards-movement the flow-field is simplified (global vortex) compared to the upwards movement.

Overall the flow-field analysis suggests that higher energy (and especially higher β) configurations cause vertically further stretched vortex structures which upon separation (as the particle changes direction) sustain longer and cause longer periods where the particle works 'against' a heading vortex in the downwards-movement. The same mechanism can be witnessed in confined domains when compared to their counterparts. The period-partition (a_{ud}) during which the particle works 'against' a heading vortex in the upwards-movement, but does not in the downwards-movement decreases with smaller domains and retardation increases. The metric also decreases throughout increases of amplitude A. The asymmetry-metric a_{ud} does, however, not collapse across material configurations (table 4.4 ID=103 vs. ID=98). Generally speaking, the occurrence and dissipation of the flow-structures mentioned can hardly be linked to visible changes in the forces eminent on the particle (figure 4.3).

				Θ_6			Θ_{10}		
ID	ρ_s[-]	β [-]	f [Hz]	$\frac{\overline{U}}{U_0}$	C_{dp}	a_{ud}[%]	$\frac{\overline{U}}{U_0}$	C_{dp}	a_{ud}[%]
26	11.4	2.6	65.9	0.72	0.47	**74**	0.79	0.47	**100**
96	11.4	10.0	60.0	0.44	0.75	**17**	0.65	0.69	**22**
98	11.4	20.0	60.0	0.33	0.92	**12**	0.45	0.72	**14**
103	2.9	20.0	60.0	0.44	0.62	**-2**	0.78	0.48	**10**

Table 4.4: C_{dp}[-] and asymmetry-factor a_{ud}[%] for the flow-field-analyzed configurations both in confined and unconfined domain. E.g. ID=96, unconfined domain: During 22% of the time of the particle-downwards-movement, the flow-field is characterized by a global vortex, hence unsymmetrical compared to the upwards-movement which is still characterized by a separated heading vortex. In the confined domain the dissipation of the heading vortex in the downwards movement occurs later and the partition of time spent in asymmetry is 6%.

4.5.4 Visualizations for the Θ_6 domain

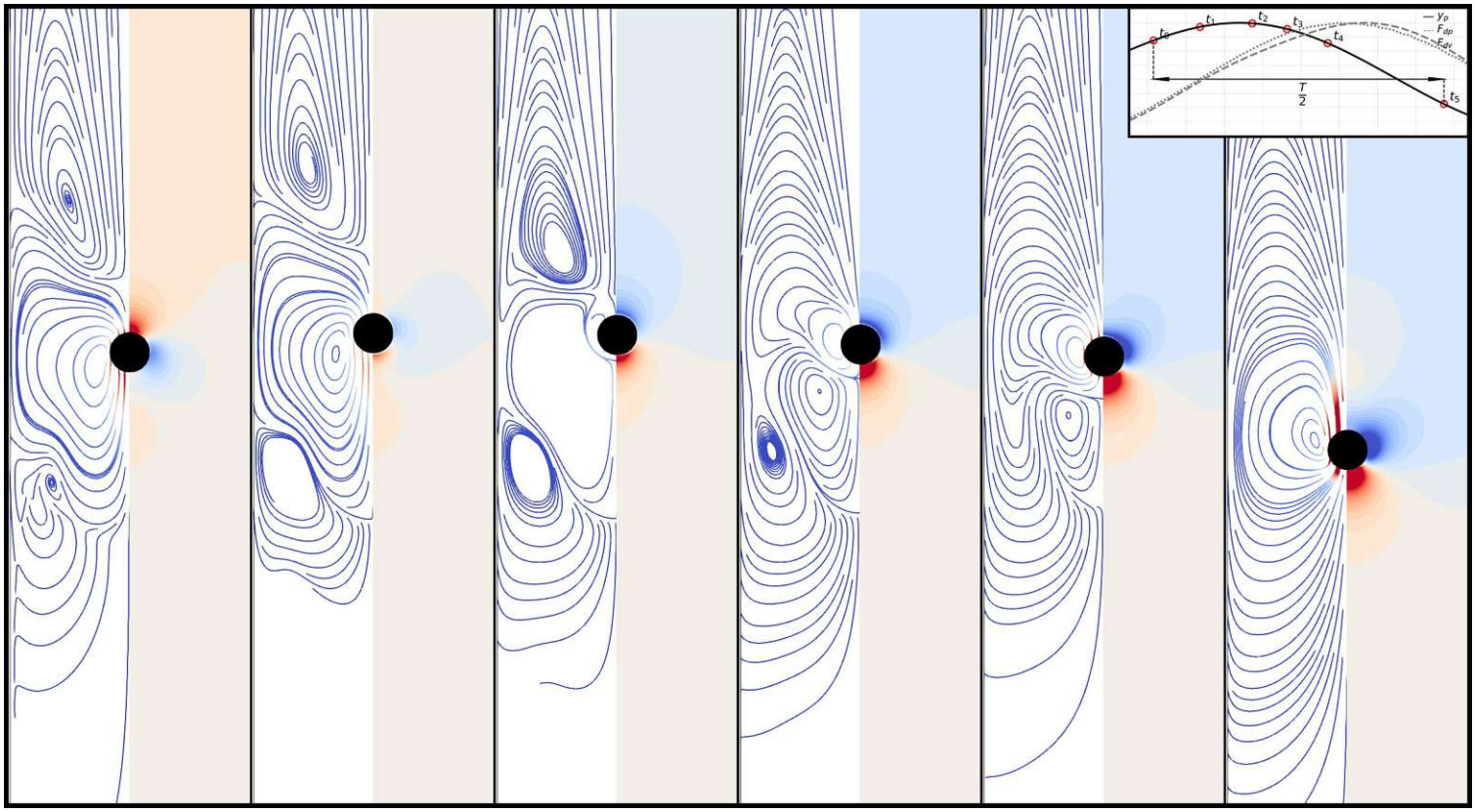

Figure 4.5: ID=26: Flow- (left) and pressure field (right) half-period.

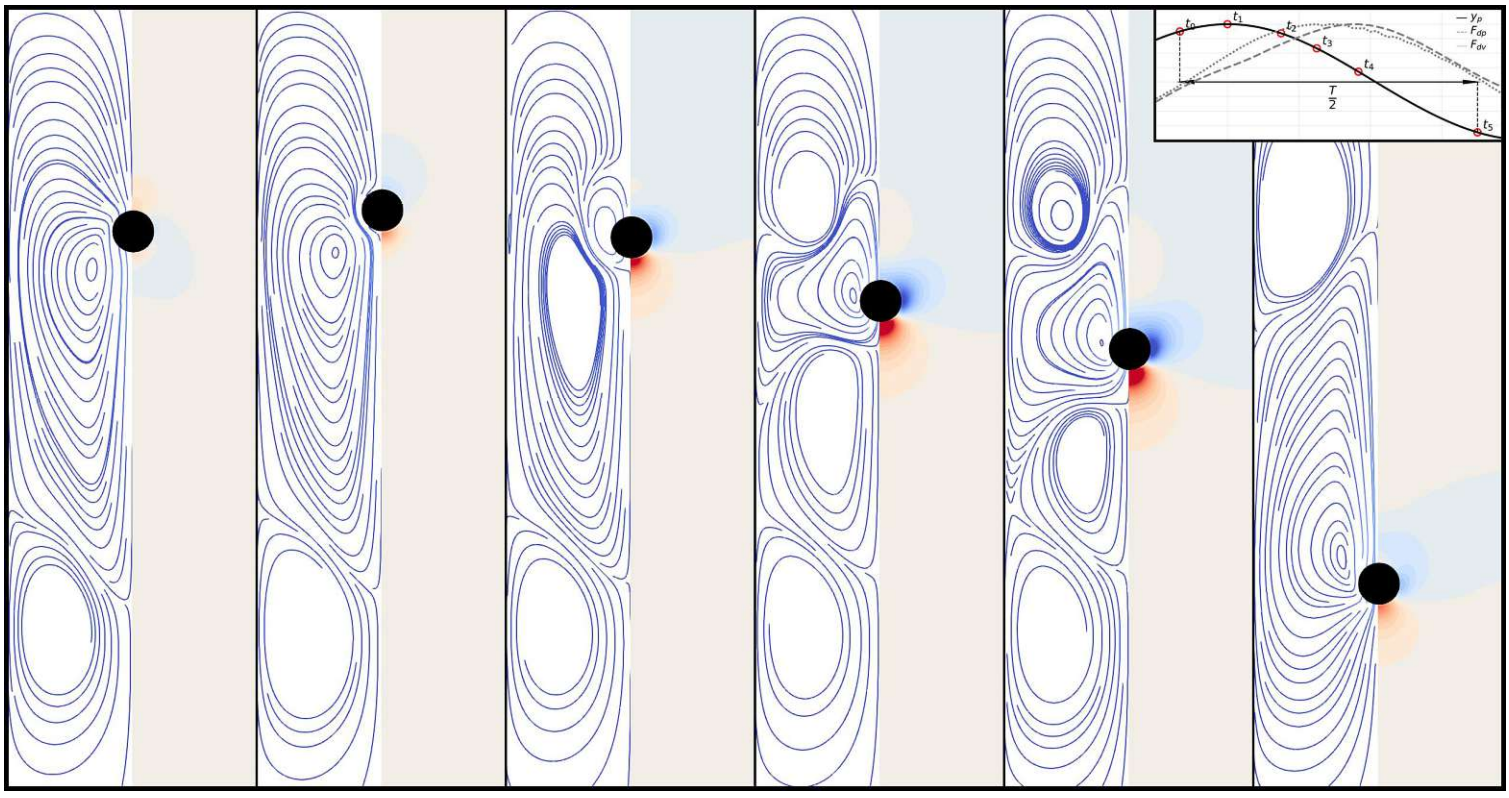

Figure 4.6: ID=103: Flow- (left) and pressure field (right) over a half-period

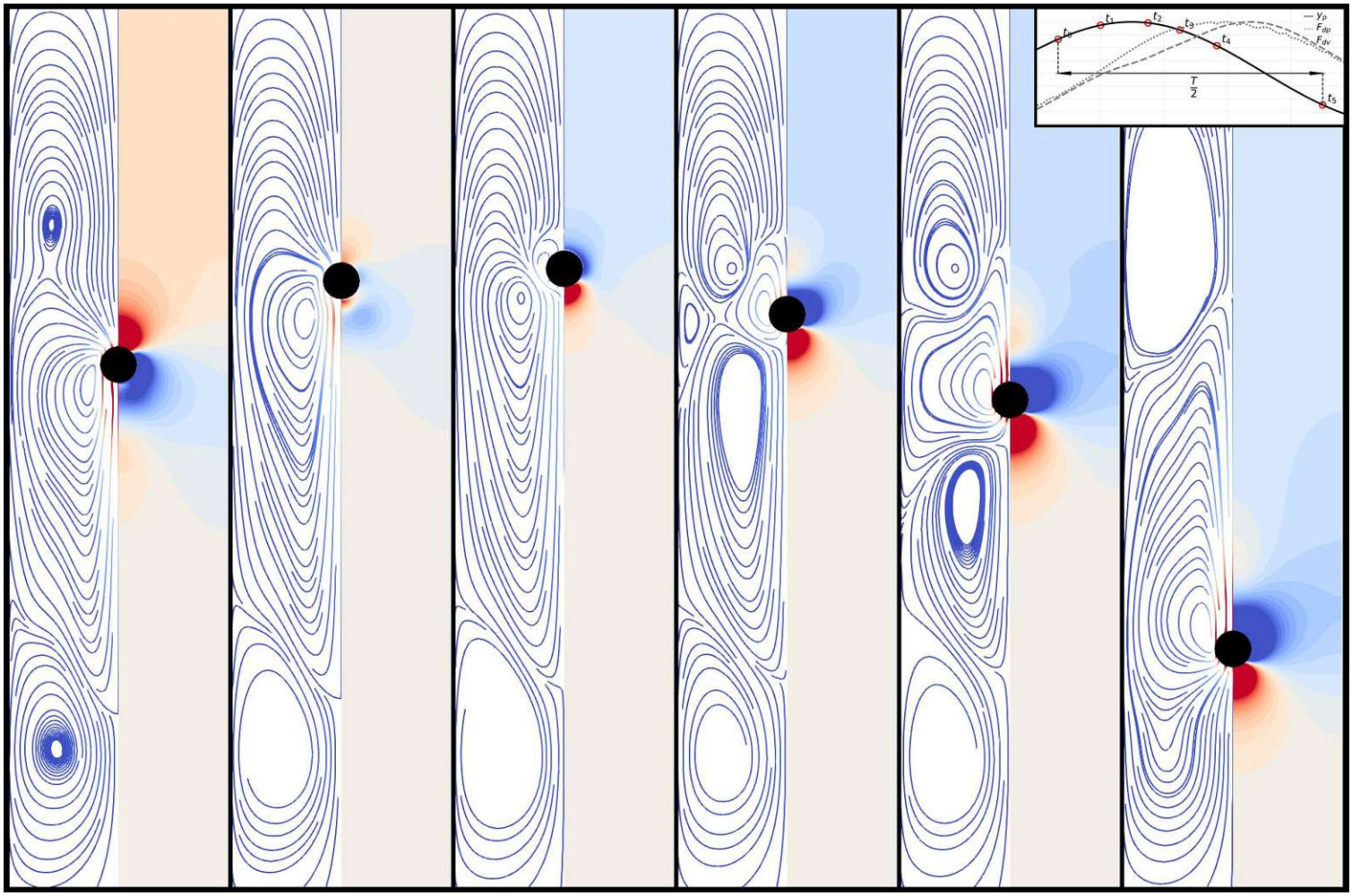

Figure 4.7: ID=96: Flow- (left) and pressure field (right) over a half-period

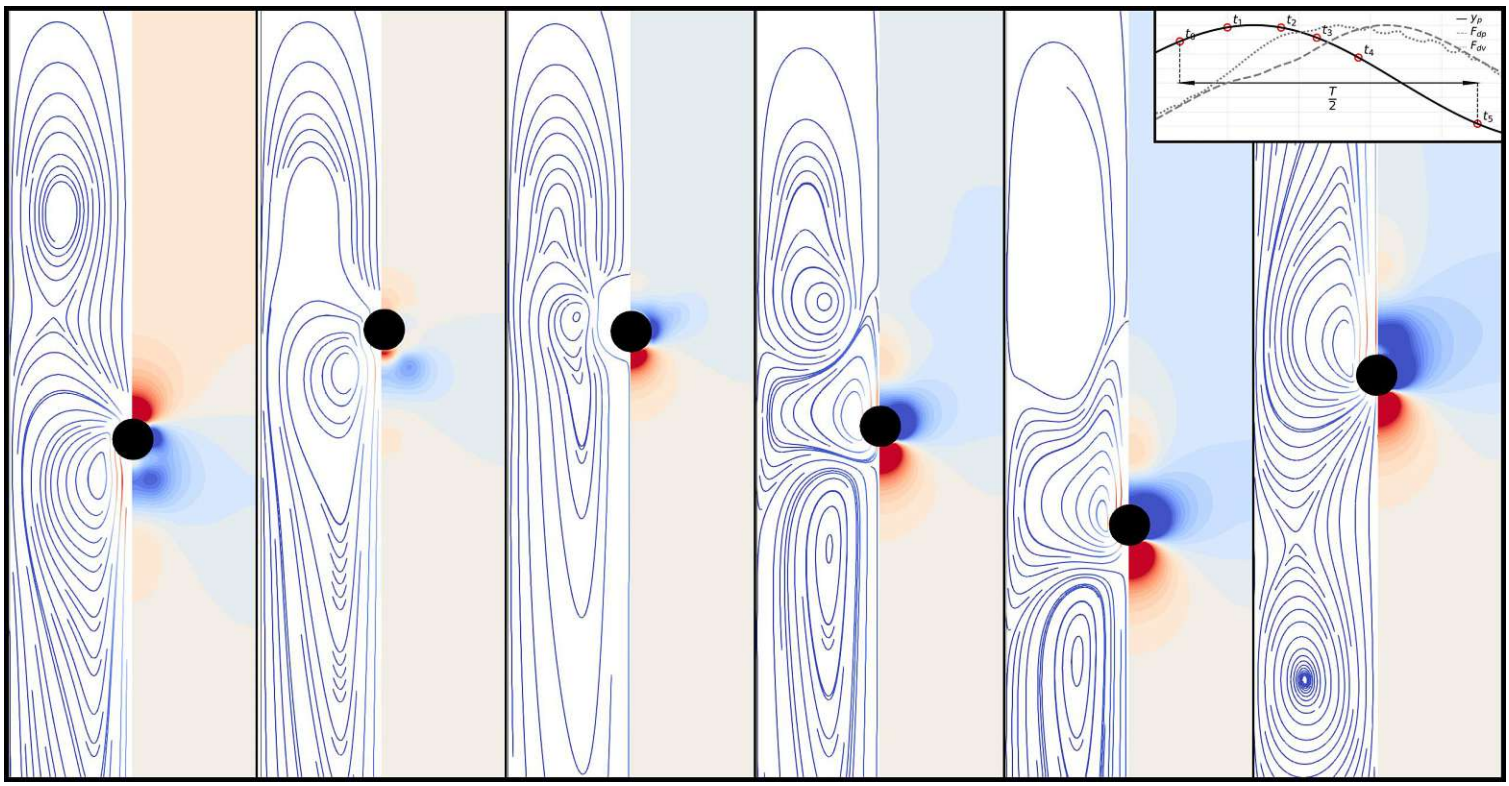

Figure 4.8: ID=98: Flow- (left) and pressure field (right) over half-period (The far right frame has been altered downwards in order to capture all flow structures)

4.5.5 Visualizations for the Θ_{10} domain

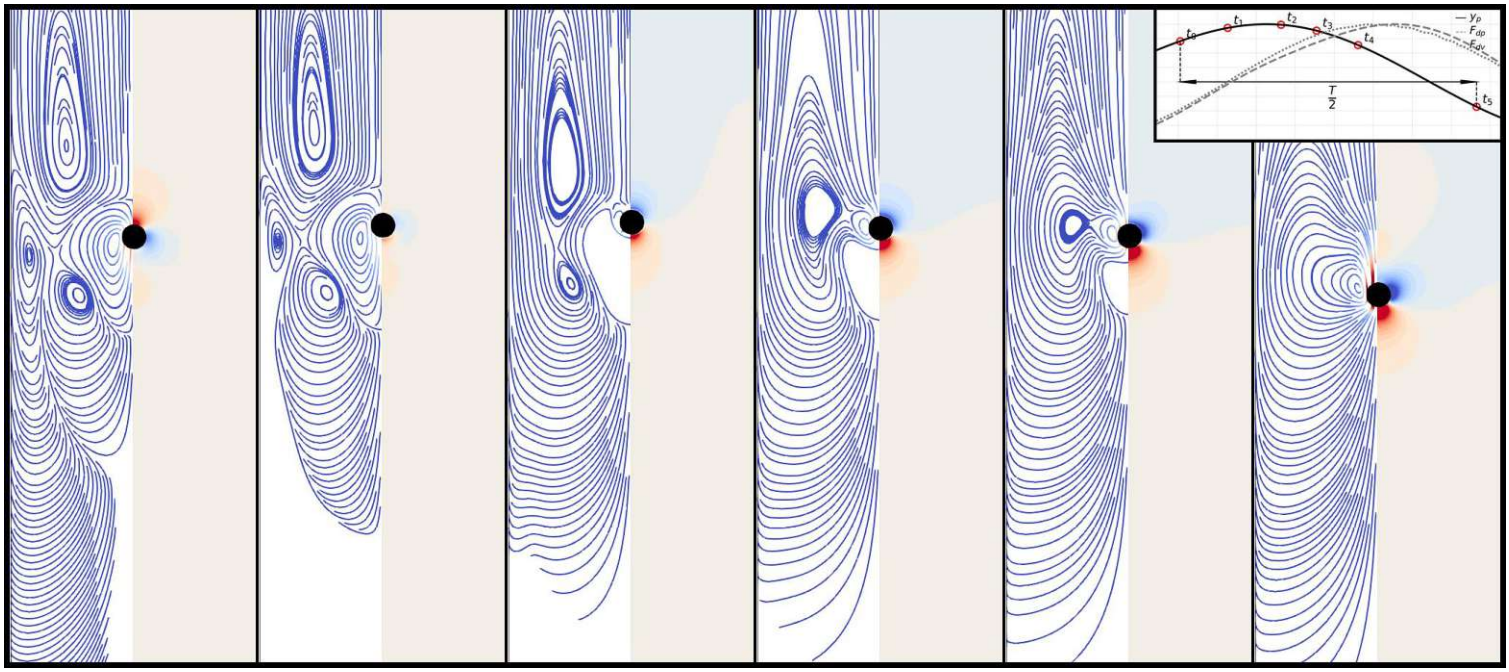

Figure 4.9: ID=26: Flow- (left) and pressure field (right) over a half-period

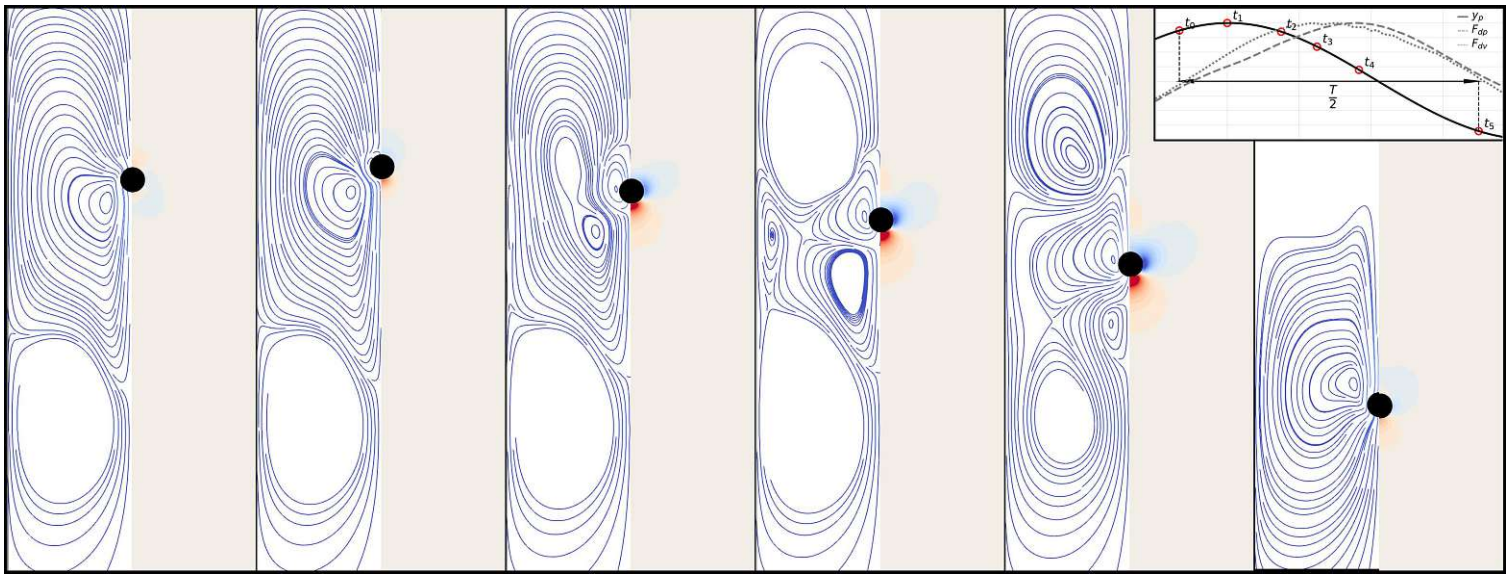

Figure 4.10: ID=103: Flow- (left) and pressure field (right) over a half-period

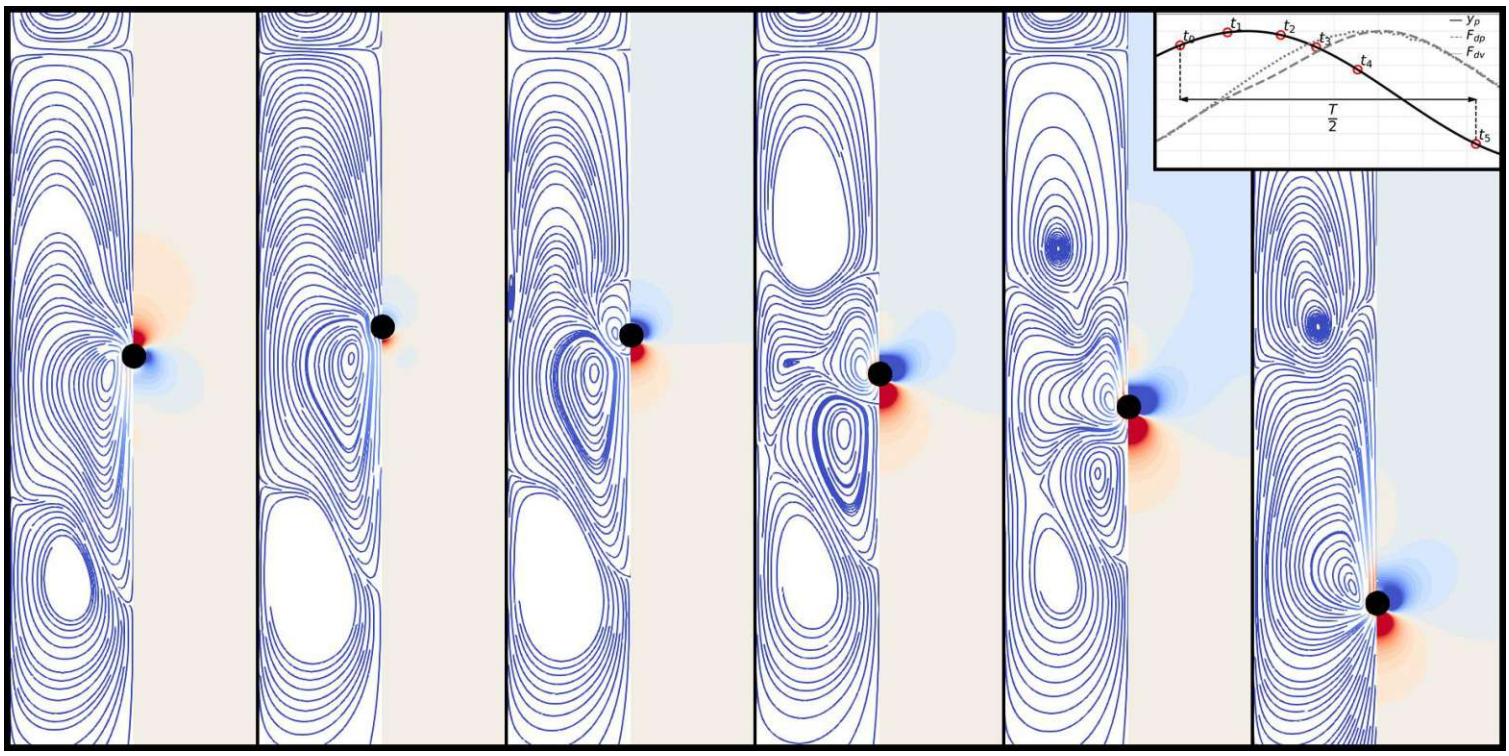

Figure 4.11: ID=63: Flow- (left) and pressure field (right) over a half-period

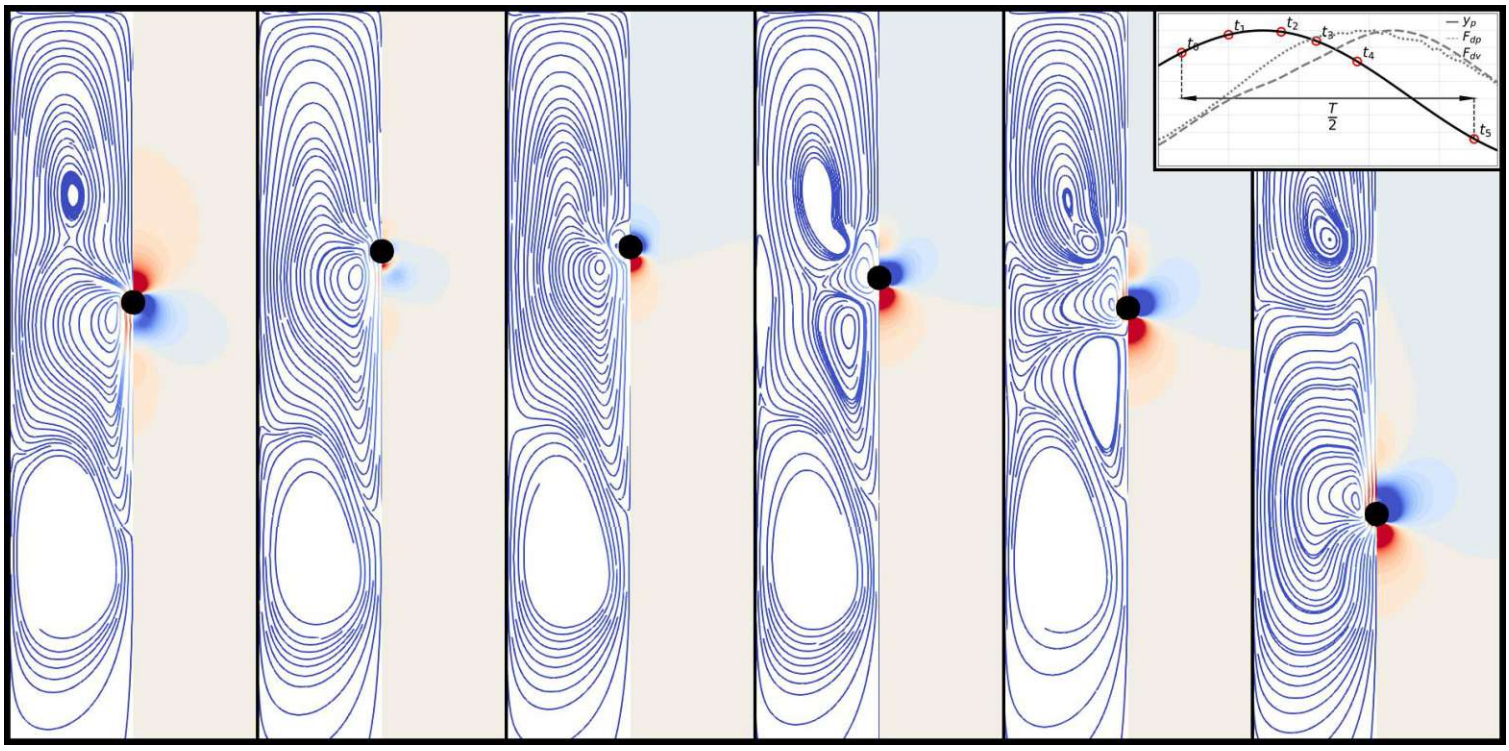

Figure 4.12: ID=96: Flow- (left) and pressure field (right) over a half-period

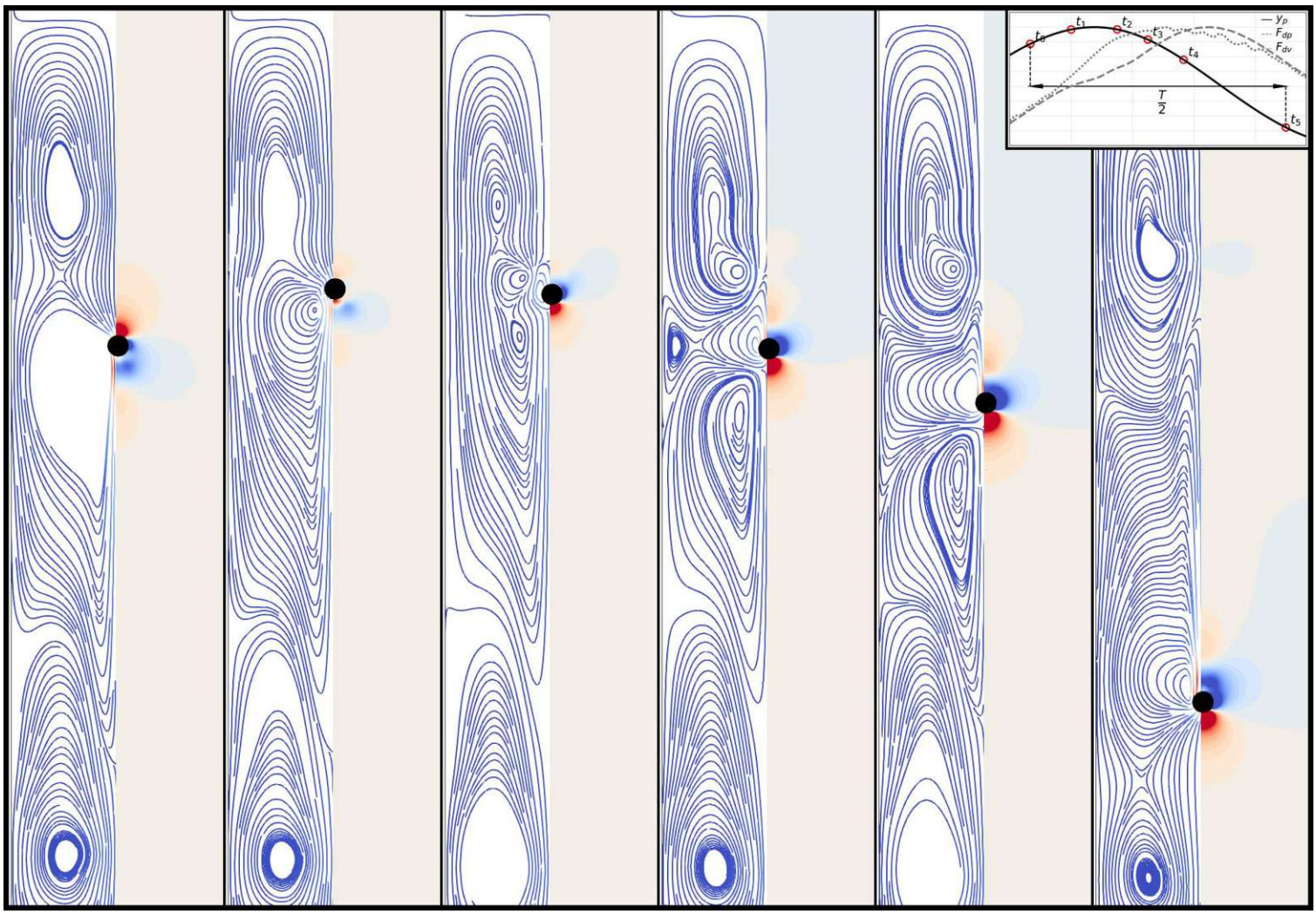

Figure 4.13: ID=98: Flow- (left) and pressure field (right) over a half-period

4.6 "Levitation"

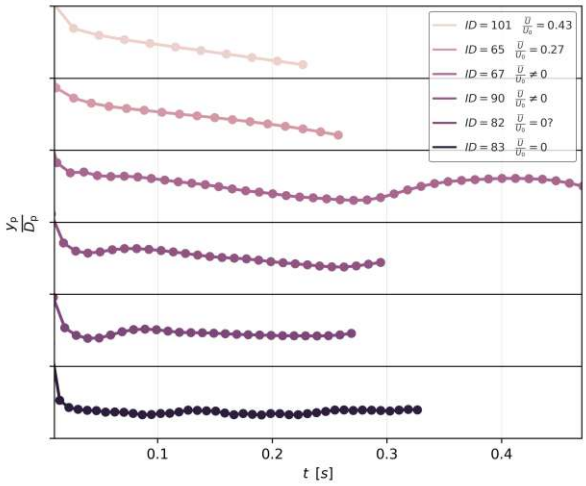

Figure 4.14: Mean particle trajectories over time for retardation configurations ID=$\{101, 65, 67, 90, 82, 83\}$ (constant oscillation amplitude $A = 20D_p$, increasing oscillation frequency $f[Hz] = \{45, 65, 85, 94, 100, 125\}$ from top to bottom) for the Θ_6 domain. Trajectories for the Θ_{10} domain are qualitatively similar.

In section 4.3 oscillation-configurations that do not result in quasi-steady particle settling were mentioned. They are highlighted (*) in tables 5.3, 5.2. Despite occurrence of very strong retarding effects, their unsteadiness forbids to compute a numeric measure for retardation magnitude $\frac{\overline{U}}{U_0}$ as proposed in section 3.5. We remain with a qualitative description. Figure 4.14 illustrates how increased frequency f causes more pronounced deviations from quasi-steady settling for a fixed material configuration. While for the configuration ID=101 ($f = 45$Hz) the quasi-steady model is well intact (linear mean trajectory), secondary effects become apparent for higher frequency settings. An outstanding feature is the 'wobble' the particle follows (most prominent throughout ID=67-82): When close to the center of the vertical span of the domain, the particle seems to be re-suspended, almost causing secondary oscillations along the trajectory. The initial 'wobble' (right after the particle is dropped) builds out with increasing f, at the same time the period length of the secondary oscillation (between 'wobbles') is decreased and the particle's loss of elevation in-between them with it. This leads to an additional delay of the collision with the bottom plate, in the extreme (ID=82,83) the particle remains suspended ('levitates') and is subject of chaotic deviations around the center of the vertical domain.

While this qualitative description was given based on a ceteris-paribus f it is important to note that similar effects have been observed for different amplitude A (same material configuration). E.g. configuration ID=66 ($A = 15D_p, f = 85Hz$) resembles the trajectory of ID=67 ($A = 20D_p, f = 65Hz$) very well (slight deviation from quasi-steady settling). On the other hand-side, not all configurations characterized by similar or greater oscillatory intensity show 'wobbly'-behaviour (ID=77 ($A = 30D_p, f = 65Hz$)). High-frequency simulations devour more computational resources and our data on configurations in this realm is therefore weak, we do however hypothesize that such unsteady configurations exists for most material configurations (especially those with large ρ_s, as they enable large particle oscillation amplitudes).

4.7 Dimensionless correlations

Following prior contributions we want to make a new attempt on relating the results obtained to a dimensionless parameter. Figure 4.4 demonstrated that retardation scales well with parameters based on the pressure contribution to the net-lift (e.g. C_{dp}). Parameters proposed by Baird [BST04], Wang [Hwa85] and Schöneborn [Sch75] are based on a Strouhal number (that demands knowledge about the terminal settling velocity U_0 and/or the frequency for which natural vortex shedding occurs f_{nvs}). This information can in parts be gathered from prior experiments on the material configuration in question, but it makes use of these parameters unhandy. Only Herringe's [Her76] dimensionless parameter $\beta\sqrt{\frac{v}{D_p^2\omega}}$ is based solely on material and oscillation parameters.

Correlations presented in figure 4.15 hold data from our simulations, as well as the experimental Herringe data-set. Additionally, results reported by Tunstall and Houghton [TH09], as well as Ho [Ho01] (whose experimental set-ups are in line with the one employed numerically and are described in section 3.4) were extracted. Due to the low-viscosity fluids employed in the corresponding experiments (table 5.1) both sets are rich in configurations characterized by very high Reynolds numbers ($Re > 1e^3$), setting them apart from the numerical results gathered during this study.

The correlation parameter proposed by Herringe has a strong correlation with the oscillation Reynolds number Re_ω. Both collapse retardation magnitude $\frac{\overline{U}}{U_0}$ well, as long as all data stems from a similar material configuration. Data obtained from low viscosity fluid setups (high Re) and data with much higher viscosity set-ups are not brought together well. Even though it shares most input parameters (ω, ν) the Stokes number St presents itself as a considerably worse choice to describe the system, when compared to Re_ω. While Re_ω relies on the amplitude A as length-scale, St is based on the particle-diameter D_p, we conclude that the former is the dominant length-scale in the problem. This is in line with Baird's study on pulsed flow past a cylinder in which he states that, if oscillations are intended to increase drag, it is generally more effective to use a high amplitude and low frequency than to use a low amplitude and a high frequency [Bai67]. The peculiar Strouhal number

$$Sr = \frac{A\omega}{u_{\text{fall}}}$$

we define relies on an estimate for the settling velocity $u_{\text{fall}} = \sqrt{D_p g(1 - \frac{1}{\rho_s})} \approx U_0$ in a quiescent fluid, by modelling the particle's buoyancy-corrected velocity after free-fall-length D_p (Modelling via Stokes-velocity leads causes lesser collapse). Sr also relies on the approximation that all configurations are inertial enough to force $f_{nvs} = f$ (per mechanism described in section 1.3). It leads to much better collapse than the parameters aforementioned.

The parameter $\chi = \rho_s^a Re_\omega^b \Gamma^c = \rho_s^2 Re_\omega^1 \Gamma^{\frac{1}{2}}$ we put forward is based on the parameters from the dimensional analysis in section 3.3 and fitted to the data. It shares the ability to pool low-β configurations to the upper left corner of the plot much more consistently with the Sr parameter. Because the parameter-grid in this study was not designed to deliver extensive ceteris-paribus sweeps of the three parameters ρ_s, Re_ω and Γ (which generally is hard since the latter two both depend on viscosity) we gained too little data for a parametric study on those parameters. The

weights a, b, c that enable the best fit, attribute similar importance to the density ratio rho_s as to the oscillation amplitude A (squared in the Re_ω parameter). While our simulations cover only two density-ratios, the experimental data (which also collapses over χ) hold many more. The configuration pairs fulfilling ceteris-paribus ρ_s- alteration (e.g. ID=$\{33, 96\}, \{41, 98\}$) support the strong influence of the parameter. Increasing ρ_s causes stronger retardation ($\Delta \frac{\overline{U}}{U_0}_{10}$ = 20-40% for the Θ_{10}- and $\Delta \frac{\overline{U}}{U_0}_{6}$ = 15% for the Θ_6 domain for threefold increase of ρ_s)

The collapse for data obtained from the Θ_{10}- and the Θ_6 domain in figure 4.15 illustrate that low ρ_s-configurations are affected most by a confined domain (note that the experimental data points are similar in plots corresponding to both domains and are one from unconfined domain, this observation is therefore based on the simulation results for the $\rho_{s0} = 2.96$ configurations). While the $\rho_{s26} = 11.4$ configurations experience a general shift towards lower retardation (numerically illustrated in table 4.4) upon domain-span-expansion, the ρ_{s0} configurations loose their collapsed formation in addition to a drastic decrease of retardation (visible in Sr, χ-plots).

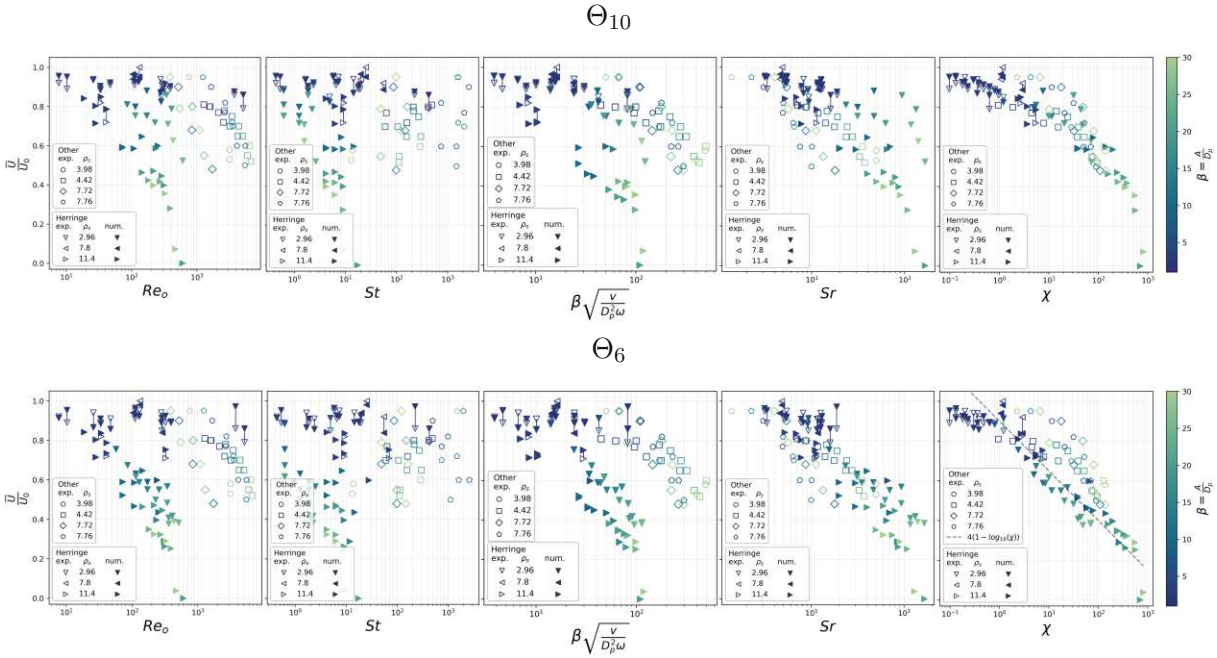

Figure 4.15: Dimensionless correlation of retardation magnitude over a combination of parameters obtained by dimensional analysis (section 3.3). Marker-form indicates ρ_s and marker-color indicates β. Filled markers represent numerical results, while empty ones represent experimental data. Vertical lines (between filled an unfilled markers) show the error between numerical simulation and the original experiment.

CHAPTER 5

Conclusion

1. We investigated the physical mechanism causing particle retardation. We found a strong link between retardation magnitude $\overline{U}/U_0$ and the contribution of the pressure force to the net-lift (C_{dp}) (figure 4.4). This contribution is caused by an increasing asymmetry in the pressure force F_{dp} and scales with the 'delay' of F_{dp} relative to the viscous drag F_{dv} (ϕ_{vp}). We also discovered a pattern indicating differences in flow-structures during particle-upwards movement compared to the downwards movement over an oscillation half-period as discussed in section 4.5. (The partition of a half-period (a_{ud}) throughout which the particle is not moving against a separated vortex during the downwards- movement, compared to the partition throughout which the particle is moving against such a vortex during the upwards-movement, scales indirectly with retardation (within a material configuration)). We suspect this flow field asymmetry to occur stronger in configurations where gravity is dominant compared to the oscillation-induced effects. We were not able to link significant changes of the flow field to the magnitude of the hydro-static force F_h on the particle or the 'delay' between its components F_{dp} and the viscous drag F_{dv}. However, since the absolute magnitude of the hydro-static force F_h is by orders larger than the asymmetry in upwards- compared to downwards-movement ($\approx F_{hmax} - F_{hmin}$), even a slight increase in pressure force during the particle-upwards movement compared to the down-wards movement can compound over oscillations and have a significant effect on net-lift.

2. The influence of a confined horizontal domain on particle retardation was explored. It was found that a confined test domain generally leads to greater retardation. The confinement effects are fond to become more prominent if the viscosity is increased. Additionally, configurations with low density-ratio ρ_s were found to be especially sensitive to confinement. Confining the system from a horizontal cross section of $10D_p \times 10D_p$ (Θ_{10}) to a $6D_p \times 6D_p$ (Θ_6) was found to result in an increase in retardation by as much as 20%. Interestingly, the magnitude of reactionary forces F_{dp}, F_{dv} eminent on a particle (figure 4.3) is almost unaffected by this confinement. At the same time the flow-field is visibly affected and the asymmetry factor a_{ud} decreases with decreased horizontal domain span. Hence, symmetrical flow-field-conditions (with respect to the particle's up- and downwards movement) are sustained throughout a longer period of the half-period.

3. We found a configurations (ID=83) for which particle levitation, as an extreme case of retardation in a single-particle system, was observed. The particle settling behaviour

observed does not suffice the quasi-steady criterion (the particle velocity oscillates around a terminal mean settling velocity $\overline{U}$). Instead the particle engages in chaotic deviations around the middle of the vertical domain span (figure 4.14). This geometrical aspect suggests that the effect might be caused by the limited vertical domain span employed in the simulations. However, the wobbly particle trajectory is reminiscent of the descriptions Feinman [Fei01] gave about chaotic particle-levitation he witnessed in multi-particle systems. The differences between multi-particle and single-particle system remain unclear.

4. An approximated Strouhal number $Sr = \frac{D_p f}{u_{\text{fall}}}$ was found to yield good collapse for experimental and numerical retardation data across a wide range of material and oscillation parameters. Through comparison of collapses obtained from Stokes number St, which depends on the particle diameter D_p as length-scale, and oscillation Reynolds number Re_ω, which depends on the oscillation amplitude A, the amplitude A was found to be the predominant length-scale. A more complex dimensionless parameter χ, constructed from parameters obtained by dimensional analysis, was fitted to achieve much better collapse than prior suggestions. It is composed with a previously unconsidered parameter $\Gamma = \frac{gD_p^3}{\nu^2}$ which relates gravitational to viscous forces.

Nomenclature

Forces

F_{rigid} force on particle due to transient motion

F_c collision force

F_e buoyancy-corrected oscillation force

F_g gravity force

F_h hydrostatic force

F_o oscillation force

F_{dp} pressure contribution to F_{dp}

F_{dv} viscous drag contribution to F_h

F_{IBM} force on particle as computed by IBM

Dimensionless entities

$\beta = \frac{A}{D_p}$ amplitude ratio

$\chi = \rho_s^2 Re_\omega \Gamma^{\frac{1}{2}}$ combined correlation parameter

$\frac{\overline{U}}{U_0}$ retardation magnitude

$\Gamma = \frac{gD_p^3}{\nu^2}$ gravitational to viscous forces

ϕ_y phase-shift between F_e and y_p

ϕ_h phase-shift between F_e and F_h

ϕ_{vp} delay between pressure and viscous component of F_h

$a = 1 - (\frac{t_{\text{vcu}} - t_{\text{vcd}}}{\frac{T}{2}})$ asymmetry-metric for flow-field in upwards versus downwards movement, where $t_{\text{vcu/d}}$ mark the point in time when the heading vortex dissipates during particle-upwards/downwards-movement

$C_{dp} = \int_T \frac{F_{\text{dp}}}{F_{\text{g}}}$ retardation magnitude

$Re = \frac{AD_p\omega}{\nu}$ Reynolds number (as obtained from non-dimensionalisation)

$Re_p = \frac{D_p u_{\max}}{\nu}$ particle Reynolds number (based on maximum particle velocity)

$Re_\omega = \frac{A^2\omega}{\nu}$ oscillation Reynolds number

$Sr = \frac{D_p f}{u_{\text{fall}}}$ approximated Strouhal number

$Sr_f = \frac{D_p f}{U_0}$ forced Strouhal number

$Sr_n = \frac{D_p f_{\text{nvs}}}{U_0}$ natural Strouhal number

$St = (\rho_s - 1)\frac{D_p^2\omega}{18\nu}$ Stokes number

Dimensional entities

ν kinematic viscosity

ρ_f fluid density

ρ_p particle density

$\Theta_{6,10}$ simulation domains with L_x=L_z=$\{6,10\}D_p$

A box oscillation amplitude

D_p particle diameter

f box oscillation frequency

h grid spacing

$L_{x,y,z}$ domain span in direction x, y, z

$w = 2\pi f$ box angular velocity

y_p particle elevation

Physics constants

g gravitational constant

Velocities

$\overline{U}$ mean settling velocity

u fluid velocity

U_0 settling velocity in quiescent fluid

$u_{\text{fall}} = \sqrt{D_p g(1 - \frac{1}{\rho_s})}$ approximation to U_0

u_{pmax} maximum velocity measured throughout a particle oscillation

$u_f = A\omega sin(\omega t)$ box velocity

u_p particle velocity

Bibliography

[ATC71] M Al-Taweel, Adel and F Carley, James. Dynamics of single spheres in pulsated flowing liquids: Part i. experimental methods and results. In *AI Ch. E. Symp. Ser*, volume 67, pages 114–123, 1971.

[Bai67] M.H.I. Baird. Some observations on pulsed flow past a cylinder. *Chemical Engineering Science*, 22(7):1056–1057, 1967.

[Bai03] JE Bailey. Particle motion in rapidly oscillating flows. *Chemical Engineering Science*, 29(3):767–773, 1974-03.

[Bie18] Edward Biegert. Eroding uncertainty: Towards understanding flows interacting with mobile sediment beds using grain-resolving simulations. 2018.

[Boy20] L Boyadzhiev. On the movement of a spherical particle in vertically oscillating liquid. *Journal of Fluid Mechanics*, 57(FEB20):545–548, 1973-02-20.

[BST04] MHI Baird, MG Senior, and RJ Thompson. Terminal velocities of spherical particles in a vertically oscillating liquid. *Chemical Engineering Science*, 22(4):551–, 1967-04.

[BVM17] Edward Biegert, Bernhard Vowinckel, and Eckart Meiburg. A collision model for grain-resolving simulations of flows over dense, mobile, polydisperse granular sediment beds. *Journal of Computational Physics*, 340:105–127, July 2017.

[Car10] Accelerated motion of a spherical particle. *Eos, Transactions American Geophysical Union*, 33(5), 1952-10.

[CLP82] W.D. Curtis, J.David Logan, and W.A. Parker. Dimensional analysis and the pi theorem. *Linear Algebra and its Applications*, 47:117–126, 1982.

[DK90] Yong Deng and Mooson Kwauk. Levitation of discrete particles in oscillating liquids. *Chemical Engineering Science*, 45(2):483–490, 1990.

[Fei01] Jerome Feinman. *An experimental study of the behavior of solid spheres in oscillating liquids*. 1964-01-01.

[Ger66] J. H. Gerrard. The mechanics of the formation region of vortices behind bluff bodies. *Journal of Fluid Mechanics*, 25(2):401–413, 1966.

[Her76] R.A. Herringe. On the motion of small spheres in oscillating liquids. *The Chemical Engineering Journal*, 11(2):89–99, 1976.

[HKHK01] Samer Hassan, Masahiro Kawaji, Samer Hassan, and Masahiro Kawaji. The effects of vibrations on particle motion in a viscous fluid cell. *Journal of Applied Mechanics*, 75(3), 2008-05-01.

[Ho01] Hau-Wong Ho. *PhD thesis: Fall velocity of a sphere in a field of oscillating fluid.* 1964-01-01.

[Hou63] Gerald Houghton. The behaviour of particles in a sinusoidal velocity field. *Proceedings of the Royal Society of London. Series A. Mathematical and Physical Sciences*, 272:33 – 43, 1963.

[Hou04] Gerald Houghton. Particle trajectories and terminal velocities in vertically oscillating fluids. *The Canadian journal of chemical engineering.*, 44(2), 1966-04.

[Hou04] Gerald Houghton. Particle retardation in vertically oscillating fluids. *The Canadian journal of chemical engineering.*, 46(2), 1968-04.

[Hwa85] Paul A. Hwang. Fall velocity of particles in oscillating flow. *Journal of Hydraulic Engineering*, 111(3):485–502, 1985.

[KCA11] William B Krantz, James F Carley, and Adel M Altaweel. Levitation of solid spheres in pulsating liquids. *Industrial Engineering Chemistry Fundamentals*, 12(4):391–396, 1973-11.

[KF12] Tobias Kempe and Jochen Fröhlich. An improved immersed boundary method with direct forcing for the simulation of particle laden flows. *Journal of Computational Physics*, 231(9):3663–3684, 2012.

[Lap56] Ch E Lapple. Fluid and particle mechanics. 1956.

[Mac92] The mixing and separation of particle suspensions using oscillatory flow in baffled tubes. *Chemical Engineering Research Design*, 71(6):649–656, 1992.

[NMH+03] X. Ni, M.R. Mackley, A.P. Harvey, P. Stonestreet, M.H.I. Baird, and N.V. Rama Rao. Mixing through oscillations and pulsations—a guide to achieving process enhancements in the chemical and process industries. *Chemical Engineering Research and Design*, 81(3):373–383, 2003. Oil and Natural Gas Production.

[OH64] Fuat Odar and Wallis S. Hamilton. Forces on a sphere accelerating in a viscous fluid. *Journal of Fluid Mechanics*, 18(2):302–314, 1964.

[OHU+10] Tatsuya Oki, Taeko Hazumi, Yoko Umemiya, Mikio Kobayashi, Tatsuya Oki, Taeko Hazumi, Yoko Umemiya, and Mikio Kobayashi. Influence of water pulsation with different frequency and amplitude on orbit of a particle placed on a fixed screen. *Materials Transactions*, 51(1):156–164, 2010.

[OKO+ 3] Tatsuya Oki, Mikio Kobayashi, Shuji Owada, Daiki Matsuura, Tatsuya Oki, Mikio Kobayashi, Shuji Owada, and Daiki Matsuura. Alteration of the equal settling ratio of fine particles by vertically-oscillating water. *International journal of mineral processing*, 82(2):69–79, 2007-3.

[PC16] Fernando Pita and Ana Castilho. Influence of shape and size of the particles on jigging separation of plastics mixture. *Waste Management*, 48:89–94, 2016.

[Sch75] P.-R. Schöneborn. The interaction between a single particle and an oscillating fluid. *International Journal of Multiphase Flow*, 2(3):307–317, 1975.

[SS09] Saverio E. Spagnolie and Michael J. Shelley. Shape-changing bodies in fluid: Hovering, ratcheting, and bursting. *Physics of Fluids*, 21:013103, 2009.

[TH09] EB Tunstall and G Houghton. Retardation of falling spheres by hydrodynamic oscillations. *Chemical Engineering Science*, 23(9):1067–, 1968-09.

[Uhl05] Markus Uhlmann. An immersed boundary method with direct forcing for the simulation of particulate flows. *Journal of computational physics*, 209(2):448–476, 2005.

[VBLFM19] Bernhard Vowinckel, Edward Biegert, Paolo Luzzatto-Fegiz, and Eckart Meiburg. Consolidation of freshly deposited cohesive and noncohesive sediment: Particle-resolved simulations. *Phys. Rev. Fluids*, 4:074305, Jul 2019.

[VWLFM19] B. Vowinckel, J. Withers, Paolo Luzzatto-Fegiz, and E. Meiburg. Settling of cohesive sediment: particle-resolved simulations. *Journal of Fluid Mechanics*, 858:5–44, 2019.

Tables

ID	$\frac{\overline{U}}{U_0}_{\text{exp}}$ [-]	$\frac{\overline{U}}{U_0}_{\text{num}}$ [-]	err_{num} [-]	ρ_s [-]	ν [$\frac{kgm^2}{s}$]	D [mm]	β [-]	f [Hz]	Re [-]	Re_p [-]	origin
Tunstall/Houghton Data-Set											
/	**0.58**	/	/	3.98	9.55E-07	0.79	76.2	10.0	**3158**	/	page 1075
/	**0.53**	/	/	3.98	9.55E-07	0.79	50.8	15.0	**3158**	/	page 1075
/	**0.80**	/	/	4.42	9.55E-07	1.58	6.3	15.0	**1559**	/	const. f study
/	**0.78**	/	/	4.42	9.55E-07	1.58	10.8	15.0	**2650**	/	const. f study
/	**0.75**	/	/	4.42	9.55E-07	1.58	13.9	15.0	**3429**	/	const. f study
/	**0.70**	/	/	4.42	9.55E-07	1.58	17.7	15.0	**4364**	/	const. f study
/	**0.65**	/	/	4.42	9.55E-07	1.58	20.3	15.0	**4988**	/	const. f study
/	**0.55**	/	/	4.42	9.55E-07	1.58	24.1	15.0	**5923**	/	const. f study
/	**0.52**	/	/	4.42	9.55E-07	1.58	27.2	15.0	**6702**	/	const. f study
/	**0.60**	/	/	4.42	9.55E-07	1.58	38.8	10.0	**6370**	/	const. $A\omega^2$ study
/	**0.65**	/	/	4.42	9.55E-07	1.58	17.2	15.0	**4246**	/	const. $A\omega^2$ study
/	**0.70**	/	/	4.42	9.55E-07	1.58	9.7	20.0	**3185**	/	const. $A\omega^2$ study
/	**0.72**	/	/	4.42	9.55E-07	1.58	6.2	25.0	**2548**	/	const. $A\omega^2$ study
/	**0.77**	/	/	4.42	9.55E-07	1.58	4.3	30.0	**2123**	/	const. $A\omega^2$ study
/	**0.80**	/	/	4.42	9.55E-07	1.58	2.4	40.0	**1592**	/	const. $A\omega^2$ study
/	**0.81**	/	/	4.42	9.55E-07	1.58	1.6	50.0	**1274**	/	const. $A\omega^2$ study
Ho Data-Set											
/	**0.96**	/	/	7.72	9.55E-07	1.00	10.4	21.7	**1486**	/	page 63
/	**0.90**	/	/	7.72	9.55E-07	1.00	22.9	3.5	**520**	/	page 63
/	**0.80**	/	/	7.72	9.55E-07	1.00	37.5	3.5	**851**	/	page 63
/	**0.68**	/	/	7.72	9.55E-07	1.00	47.9	3.5	**1088**	/	page 63
/	**0.95**	/	/	7.72	9.55E-07	1.00	11.6	5.1	**387**	/	page 63
/	**0.68**	/	/	7.72	9.55E-07	1.00	25.1	5.1	**838**	/	page 63
/	**0.55**	/	/	7.72	9.55E-07	1.00	38.7	5.1	**1290**	/	page 63
/	**0.48**	/	/	7.72	9.55E-07	1.00	51.3	5.1	**1709**	/	page 63
/	**0.79**	/	/	7.72	9.55E-07	1.00	12.5	6.6	**544**	/	page 63
/	**0.48**	/	/	7.72	9.55E-07	1.00	39.8	6.6	**1730**	/	page 63
/	**0.95**	/	/	7.76	9.55E-07	3.17	3.3	3.4	**753**	/	page 61
/	**0.90**	/	/	7.76	9.55E-07	3.17	7.3	3.4	**1657**	/	page 61
/	**0.82**	/	/	7.76	9.55E-07	3.17	11.9	3.4	**2711**	/	page 61
/	**0.72**	/	/	7.76	9.55E-07	3.17	15.2	3.4	**3465**	/	page 61
/	**0.95**	/	/	7.76	9.55E-07	3.17	3.7	5.0	**1232**	/	page 61
/	**0.77**	/	/	7.76	9.55E-07	3.17	8.0	5.0	**2670**	/	page 61
/	**0.60**	/	/	7.76	9.55E-07	3.17	12.3	5.0	**4108**	/	page 61
/	**0.50**	/	/	7.76	9.55E-07	3.17	16.3	5.0	**5443**	/	page 61
/	**0.70**	/	/	7.76	9.55E-07	3.17	8.1	6.6	**3543**	/	page 61
/	**0.60**	/	/	7.76	9.55E-07	3.17	12.7	6.6	**5512**	/	page 61

Table 5.1: experimental data from Tunstall/Houghton [TH09] and Ho [Ho01]

Herringe Data-Set (Θ_{10})												
ID	$\frac{\overline{U}}{U_0}_{\text{exp}}$ [-]	$\frac{\overline{U}}{U_0}_{\text{num}}$ [-]	err_{num} [-]	ρ_s [-]	ν [$\frac{kgm^2}{s}$]	D [mm]	β [-]	f [Hz]	Re [-]	Re_p [-]	St [-]	Sr [-]
0	**0.89**	**0.88**	0.01	2.96	2.2E-05	1.00	5.9	19.9	**33**	9	0.62	7.82
1	**0.85**	**0.82**	0.03	2.96	2.6E-06	1.00	6.3	19.0	**284**	152	4.90	7.44
2	**0.89**	**0.90**	0.01	2.96	2.6E-06	1.00	2.4	68.0	**391**	218	17.90	26.68
3	**0.91**	**0.92**	0.01	2.96	2.0E-05	1.00	2.2	68.5	**47**	19	2.38	26.88
4	**0.92**	**0.89**	0.04	7.8	3.8E-06	1.00	2.0	86.8	**289**	259	54.84	29.70
5	**0.94**	**0.97**	0.03	7.8	4.1E-06	1.00	2.0	34.0	**104**	128	19.84	11.62
6	**0.94**	**0.94**	0.01	2.96	3.9E-05	1.00	1.7	95.3	**26**	9	1.66	37.38
7	**0.95**	**0.93**	0.03	2.96	3.4E-06	1.00	1.9	36.2	**129**	85	7.32	14.19
8	**0.91**	**0.93**	0.02	2.96	3.7E-06	1.00	1.9	35.5	**111**	73	6.54	13.93
9	**0.89**	**0.91**	0.03	2.96	3.3E-06	1.00	1.8	92.3	**322**	175	19.36	36.23
10	**0.94**	**0.87**	0.07	2.96	2.4E-06	1.00	2.1	50.0	**277**	170	14.39	19.61
11	**0.95**	**0.96**	0.01	2.96	2.3E-06	1.00	2.1	19.2	**112**	99	5.80	7.53
12	**0.89**	**0.90**	0.02	2.96	1.9E-05	1.00	2.0	51.1	**33**	13	1.86	20.05
13	**0.89**	**0.95**	0.07	2.96	2.6E-05	1.00	2.1	20.2	**10**	3	0.53	7.93
14	**0.86**	**0.88**	0.02	2.96	4.0E-07	1.00	1.8	133.1	**374**	2103	224.98	52.21
15	**0.79**	**0.86**	0.09	2.96	2.5E-07	1.00	1.3	156.4	**511**	3064	425.35	61.38
16	**0.92**	**0.96**	0.04	2.96	5.6E-05	1.00	1.9	35.8	**8**	2	0.44	14.04
21	**1.00**	**0.95**	0.05	7.8	3.4E-06	1.00	2.0	35.5	**132**	163	24.97	12.14
26	**0.72**	**0.79**	0.09	11.4	2.6E-05	1.00	2.6	65.9	**41**	34	9.17	22.02
28	**0.82**	**0.85**	0.04	11.4	1.9E-05	1.00	2.1	49.3	**34**	32	9.39	16.46
Extension[1]												
32	/	**0.80**	/	2.96	2.2E-05	1.00	10.0	40.0	**114**	32	1.25	15.69
33	/	**0.88**	/	2.96	2.2E-05	1.00	10.0	60.0	**172**	53	1.87	23.54
35	/	**0.81**	/	2.96	2.2E-05	1.00	15.0	20.0	**86**	17	0.62	7.85
36	/	**0.75**	/	2.96	2.2E-05	1.00	15.0	40.0	**172**	44	1.25	15.69
39	/	**0.75**	/	2.96	2.2E-05	1.00	20.0	20.0	**114**	22	0.62	7.85
40	/	**0.72**	/	2.96	2.2E-05	1.00	20.0	40.0	**229**	55	1.25	15.69
41	/	**0.83**	/	2.96	2.2E-05	1.00	20.0	60.0	**343**	92	1.87	23.54
61	/	**0.60**	/	11.4	2.6E-05	1.00	10.0	105.0	**253**	184	14.62	35.10
63	/	**0.59**	/	11.4	2.6E-05	1.00	10.0	30.0	**72**	49	4.18	10.03
64	/	**0.59**	/	11.4	2.6E-05	1.00	15.0	65.0	**235**	161	9.05	21.73
65	/	**0.40**	/	11.4	2.6E-05	1.00	20.0	65.0	**313**	208	9.05	21.73
68	/	**0.71**	/	2.96	2.6E-05	1.00	25.0	60.0	**361**	87	1.57	23.54
69	/	**0.63**	/	2.96	2.6E-05	1.00	30.0	60.0	**434**	99	1.57	23.54
71	/	**0.79**	/	2.96	2.6E-05	1.00	20.0	85.0	**410**	114	2.23	33.35
72	/	**0.42**	/	11.4	2.6E-05	1.00	25.0	30.0	**181**	103	4.18	10.03
73	/	**0.40**	/	11.4	2.6E-05	1.00	30.0	30.0	**217**	119	4.18	10.03
74	/	**0.42**	/	11.4	2.6E-05	1.00	25.0	45.0	**271**	167	6.27	15.04
75	/	**0.36**	/	11.4	2.6E-05	1.00	30.0	45.0	**325**	194	6.27	15.04
76	/	**0.42**	/	11.4	2.6E-05	1.00	25.0	65.0	**392**	267	9.05	21.73
77	/	**0.07**	/	11.4	2.6E-05	1.00	30.0	65.0	**470**	316	9.05	21.73
80	/	**0.52**	/	2.96	2.2E-05	1.00	25.0	85.0	**607**	167	2.65	33.35
83	/	**0.00**	/	11.4	2.6E-05	1.00	20.0	125.0	**602**	454	17.40	41.78
96	/	**0.64**	/	11.4	2.6E-05	1.00	10.0	60.0	**145**	104	8.35	20.06
97	/	**0.46**	/	11.4	2.6E-05	1.00	20.0	30.0	**144**	87	4.18	10.03
98	/	**0.45**	/	11.4	2.6E-05	1.00	20.0	60.0	**289**	190	8.35	20.06
99	/	**0.84**	/	11.4	2.6E-05	1.00	2.60	30.0	**18**	17	4.18	10.03
100	/	**0.56**	/	11.4	2.6E-05	1.00	10.0	45.0	**108**	77	6.27	15.04
101	/	**0.47**	/	11.4	2.6E-05	1.00	20.0	45.0	**216**	139	6.27	15.04
102	/	**0.80**	/	11.4	2.6E-05	1.00	2.60	45.0	**28**	25	6.27	15.04
103	/	**0.78**	/	2.69	2.6E-05	1.00	20.0	60.0	**289**	75	1.57	23.54
67	/	**?***	/	11.4	2.6E-05	1.00	20.0	85.0	**410**	298	11.83	28.4
82	/	**?***	/	11.4	2.6E-05	1.00	20.0	100.0	**482**	357	13.92	33.4
90	/	**?***	/	11.4	2.6E-05	1.00	20.0	94.0	**453**	329	13.09	31.4
94	/	**?***	/	11.4	2.6E-05	1.00	25.0	80.0	**482**	343	11.14	26.7

Table 5.2: Numerical and experimental data from configurations according to Herringe [Her76] for the Θ_{10} domain.
[1] material properties (ν, ρ_s) from $ID = 0, 26$ oscillation properties (β, A) extended
* indicates a non-quasi-steady-state trajectory, $\frac{\overline{U}}{U_0} = ?$ unmeasureable

Herringe Data-Set (Θ_6)												
ID	$\frac{\overline{U}}{U_0}_{\text{exp}}$ [-]	$\frac{\overline{U}}{U_0}_{\text{num}}$ [-]	err_{num} [-]	ρ_s [-]	ν [$\frac{kgm^2}{s}$]	D [mm]	β [-]	f [Hz]	Re [-]	Re_p [-]	St [-]	Sr [-]
0	(**0.89**)	**0.88**	0.01	2.96	2.2E-05	1.00	5.9	19.9	**33**	9	0.62	7.82
1	(**0.85**)	**0.91**	0.07	2.96	2.6E-06	1.00	6.3	19.0	**284**	158	4.90	7.44
2	(**0.89**)	**0.90**	0.01	2.96	2.6E-06	1.00	2.4	68.0	**391**	221	17.90	26.68
3	(**0.91**)	**0.86**	0.06	2.96	2.0E-05	1.00	2.2	68.5	**47**	23	2.38	26.88
4	(**0.92**)	**0.84**	0.09	7.8	3.8E-06	1.00	2.0	86.8	**289**	258	54.84	29.70
5	(**0.94**)	**0.94**	0.00	7.8	4.1E-06	1.00	2.0	34.0	**104**	133	19.84	11.62
6	(**0.94**)	**0.87**	0.08	2.96	3.9E-05	1.00	1.7	95.3	**26**	9	1.66	37.38
7	(**0.95**)	**0.92**	0.03	2.96	3.4E-06	1.00	1.9	36.2	**129**	86	7.32	14.19
8	(**0.91**)	**0.93**	0.02	2.96	3.7E-06	1.00	1.9	35.5	**111**	74	6.54	13.93
9	(**0.89**)	**0.92**	0.04	2.96	3.3E-06	1.00	1.8	92.3	**322**	178	19.36	36.23
10	(**0.94**)	**0.89**	0.05	2.96	2.4E-06	1.00	2.1	50.0	**277**	173	14.39	19.61
11	(**0.95**)	**0.96**	0.01	2.96	2.3E-06	1.00	2.1	19.2	**112**	100	5.80	7.53
12	(**0.89**)	**0.91**	0.02	2.96	1.9E-05	1.00	2.0	51.1	**33**	13	1.86	20.05
13	(**0.89**)	**0.95**	0.07	2.96	2.6E-05	1.00	2.1	20.2	**10**	3	0.53	7.93
14	(**0.86**)	**0.97**	0.13	2.96	4.0E-07	1.00	1.8	133.1	**3740**	2103	224.98	52.21
15	(**0.79**)	**0.86**	0.09	2.96	2.5E-07	1.00	1.3	156.4	**5117**	3064	425.35	61.38
16	(**0.92**)	**0.91**	0.01	2.96	5.6E-05	1.00	1.9	35.8	**8**	2	0.44	14.04
21	(**1.00**)	**0.98**	0.02	7.8	3.4E-06	1.00	2.0	35.5	**132**	164	24.97	12.14
25	(**0.71**)	**0.75**	0.06	11.4	3.2E-06	1.00	2.7	61.3	**326**	349	69.77	20.48
26	(**0.72**)	**0.73**	0.02	11.4	2.6E-05	1.00	2.6	65.9	**41**	34	9.17	22.02
28	(**0.82**)	**0.84**	0.02	11.4	1.9E-05	1.00	2.1	49.3	**34**	32	9.39	16.46
Extension[1]												
31	/	**0.76**	/	2.96	2.2E-05	1.00	10.0	20.0	**57**	13	0.62	7.85
32	/	**0.63**	/	2.96	2.2E-05	1.00	10.0	40.0	**114**	32	1.25	15.69
33	/	**0.59**	/	2.96	2.2E-05	1.00	10.0	60.0	**172**	53	1.87	23.54
35	/	**0.67**	/	2.96	2.2E-05	1.00	15.0	20.0	**86**	17	0.62	7.85
36	/	**0.55**	/	2.96	2.2E-05	1.00	15.0	40.0	**172**	44	1.25	15.69
37	/	**0.55**	/	2.96	2.2E-05	1.00	15.0	60.0	**257**	73	1.87	23.54
39	/	**0.62**	/	2.96	2.2E-05	1.00	20.0	20.0	**114**	21	0.62	7.85
40	/	**0.50**	/	2.96	2.2E-05	1.00	20.0	40.0	**229**	55	1.25	15.69
41	/	**0.48**	/	2.96	2.2E-05	1.00	20.0	60.0	**343**	92	1.87	23.54
50	/	**0.57**	/	2.96	2.2E-05	1.00	15.0	80.0	**343**	104	2.49	31.39
51	/	**0.59**	/	2.96	2.2E-05	1.00	15.0	30.0	**129**	30	0.93	11.77
61	/	**0.44**	/	11.4	2.6E-05	1.00	10.0	105.0	**253**	183	14.62	35.10
63	/	**0.52**	/	11.4	2.6E-05	1.00	10.0	30.0	**72**	49	4.18	10.03
64	/	**0.40**	/	11.4	2.6E-05	1.00	15.0	65.0	**235**	160	9.05	21.73
65	/	**0.26**	/	11.4	2.6E-05	1.00	20.0	65.0	**313**	206	9.05	21.73
66	/	**0.29**	/	11.4	2.6E-05	1.00	15.0	85.0	**307**	215	11.83	28.41
68	/	**0.38**	/	2.96	2.6E-05	1.00	25.0	60.0	**361**	87	1.57	23.54
69	/	**0.39**	/	2.96	2.6E-05	1.00	30.0	60.0	**434**	99	1.57	23.54
70	/	**0.42**	/	2.96	2.6E-05	1.00	20.0	75.0	**361**	98	1.97	29.43
71	/	**0.42**	/	2.96	2.6E-05	1.00	20.0	85.0	**410**	114	2.23	33.35
72	/	**0.35**	/	11.4	2.6E-05	1.00	25.0	30.0	**181**	102	4.18	10.03
73	/	**0.32**	/	11.4	2.6E-05	1.00	30.0	30.0	**217**	118	4.18	10.03
74	/	**0.32**	/	11.4	2.6E-05	1.00	25.0	45.0	**271**	166	6.27	15.04
75	/	**0.29**	/	11.4	2.6E-05	1.00	30.0	45.0	**325**	192	6.27	15.04
76	/	**0.24**	/	11.4	2.6E-05	1.00	25.0	65.0	**392**	266	9.05	21.73
77	/	**0.04**	/	11.4	2.6E-05	1.00	30.0	65.0	**470**	314	9.05	21.73
80	/	**0.38**	/	2.96	2.6E-05	1.00	25.0	85.0	**512**	133	2.23	33.35
83	/	**0.00***	/	11.4	2.6E-05	1.00	20.0	125.0	**602**	454	17.40	41.78
86	/	**0.60**	/	11.4	2.6E-05	1.00	5.0	200.0	**241**	180	27.85	66.85
96	/	**0.45**	/	11.4	2.6E-05	1.00	10.0	60.0	**145**	103	8.35	20.06
97	/	**0.38**	/	11.4	2.6E-05	1.00	20.0	30.0	**145**	86	4.18	10.03
98	/	**0.33**	/	11.4	2.6E-05	1.00	20.0	60.0	**289**	189	8.35	20.06
99	/	**0.80**	/	11.4	2.6E-05	1.00	2.60	30.0	**18**	17	4.18	10.03
100	/	**0.46**	/	11.4	2.6E-05	1.00	10.0	45.0	**108**	76	6.27	15.04
101	/	**0.34**	/	11.4	2.6E-05	1.00	20.0	45.0	**216**	138	6.27	15.04
102	/	**0.71**	/	11.4	2.6E-05	1.00	2.60	45.0	**28**	25	6.27	15.04
103	/	**0.44**	/	2.69	2.6E-05	1.00	20.0	60.0	**289**	74	1.57	23.54
67	/	**?***	/	11.4	2.6E-05	1.00	20.0	85.0	**410**	296	1.14	112.91
82	/	**?***	/	11.4	2.6E-05	1.00	20.0	100.0	**482**	355	1.34	132.83
90	/	**?***	/	11.4	2.6E-05	1.00	20.0	94.0	**453**	332	1.26	124.86
94	/	**?***	/	11.4	2.6E-05	1.00	25.0	80.0	**482**	343	11.14	26.7

Table 5.3: Numerical and experimental data from configurations according to Herringe [Her76] for the Θ_6 domain.
[1] material properties (ν, ρ_s) from $ID = 0, 26$ oscillation properties (β, A) extended
* indicates a non-quasi-steady-state trajectory, $\frac{\overline{U}}{U_0} = ?$ unmeasureable